Article

Gate-tunable optical anisotropy in wafer-scale, aligned carbon nanotube films

Check for updates

Jason Lynch[1], Evan Smith[2], Adam Alfieri[1], Baokun Song[1,3], Matthew Klein[2,4], Christopher E. Stevens [2,4], Cindy Yueli Chen [5], Chavez FK. Lawrence[1], Cherie R. Kagan [1,5,6], Honggang Gu [3], Shiyuan Liu [3], Lian-Mao Peng [7], Shivashankar Vangala[2], Joshua R. Hendrickson [2] & Deep Jariwala [1]✉

Telecommunications and polarimetry both require the active control of the polarization of light. Currently, this is done by combining intrinsically anisotropic materials with tunable isotropic materials into heterostructures using complicated fabrication techniques owing to the lack of scalable materials that possess both properties. Tunable birefringent and dichromic materials are scarce and rarely available in high-quality thin films over wafer scales. Here we report semiconducting, highly aligned, single-walled carbon nanotubes (SWCNTs) over 4″ wafers with normalized birefringence and dichroism values of 0.09 and 0.58, respectively. The real and imaginary parts of the refractive index of these SWCNT films are tuned by up to 5.9% and 14.3% in the infrared at 2,200 nm and 1,660 nm, respectively, using electrostatic doping. Our results suggest that aligned SWCNTs are among the most anisotropic and tunable optical materials known and open new avenues for their application in integrated photonics and telecommunications.

Active control of the polarization of light is critical for technologies such as optical communications, integrated photonics and microscopy[1,2]. Although this is commonly done in the radio wave to terahertz regimes, actively controlling the polarization of light in the visible and near infrared remains difficult since few materials possess both optical anisotropy and highly tunable optical properties. Liquid crystals are the most commonly used of these materials, but they require physical movement to tune their interaction with light. Not only does physical movement decrease their durability, but it also limits their switching speed, which inhibits their incorporation into optical communication systems. Instead, materials whose optical properties can be tuned using external stimuli such as electric or magnetic fields are preferred in optical communication systems because of their fast-switching speed. However, the library of materials with tunable, in-plane optical anisotropy remains sparse. Even more scarce is the availability of such materials in high-quality thin films over wafer scales for practical applications.

Optical anisotropy is caused by structural asymmetries that result in the material having a complex refractive index ($\tilde{n} = n + ik$) that depends on the polarization of incident light. The asymmetry can occur as a result of either the intrinsic crystalline structure[3] or by etching/deposition anisotropic patterns in/on an isotropic material[4]. For uniaxial anisotropy, there are two directions that are symmetrical to one another, called the ordinary axes, that have the same refractive index ($\tilde{n}_{ord} = n_{ord} + ik_{ord}$). The third direction is the asymmetrical one and it is called the extraordinary axis, with a unique refractive index ($\tilde{n}_{ext} = n_{ext} + ik_{ext}$). The anisotropy is characterized by the normalized birefringence $\left(\frac{|n_{ord} - n_{ext}|}{n_{ord} + n_{ext}} \right)$ and normalized dichroism $\left(\frac{|k_{ord} - k_{ext}|}{k_{ord} + k_{ext}} \right)$.

Materials such as transition metal dichalcogenides[5], perovskites[6] and polymers[7] exhibit optical anisotropy, but the extraordinary axis is typically out of plane, which is less applicable to electro-optical systems since its effects can only be observed for light incident at extremely

[1]Electrical and Systems Engineering, University of Pennsylvania, Philadelphia, PA, USA. [2]Sensors Directorate, Air Force Research Laboratory, Wright-Patterson AFB, OH, USA. [3]State Key Laboratory of Intelligent Manufacturing Equipment and Technology, Huazhong University of Science and Technology, Wuhan, China. [4]KBR Inc., Beavercreek, OH, USA. [5]Department of Chemistry, University of Pennsylvania, Philadelphia, PA, USA. [6]Department of Materials Science and Engineering, University of Pennsylvania, Philadelphia, PA, USA. [7]Key Laboratory for the Physics and Chemistry of Nanodevices and Center for Carbon-based Electronics, School of Electronics, Peking University, Beijing, China. ✉e-mail: dmj@seas.upenn.edu
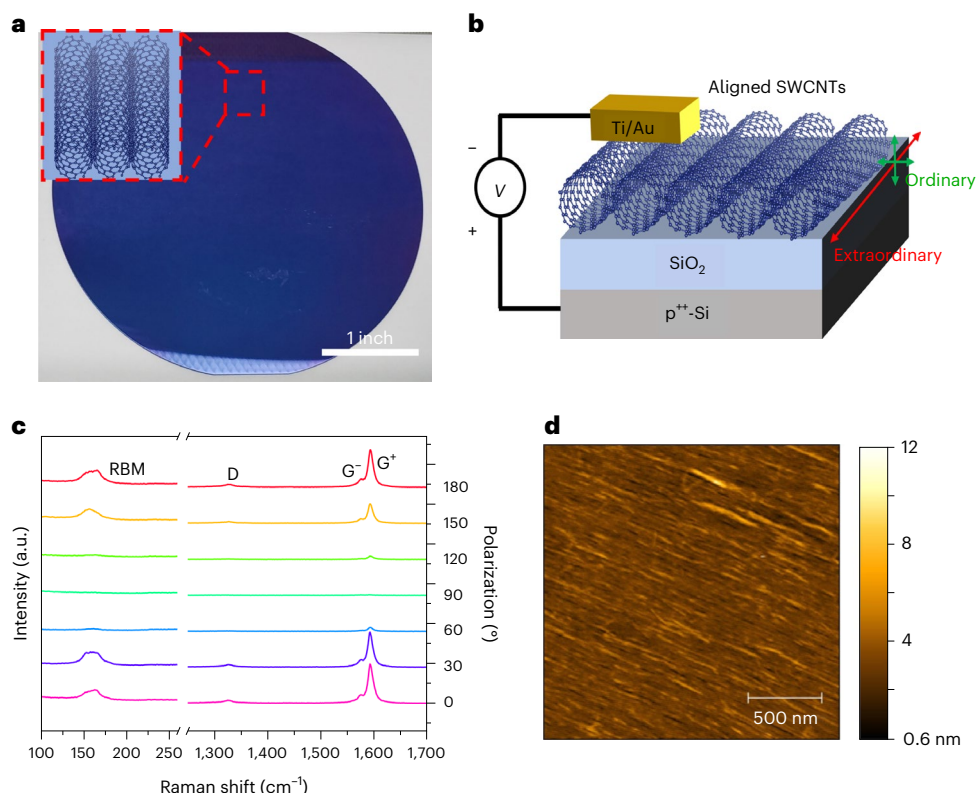
Fig. 1 | Characterization of aligned SWCNT films. a, Photograph of a 4 inch wafer with globally aligned, high-purity (99.9999%) semiconducting SWCNTs prepared using a multiple dispersion and sorting process. Inset: the direction of global alignment. **b**, Diagram of MOSCap geometry that enables the injection of holes and electrons into the SWCNT films by applying negative and positive voltages, respectively. The extraordinary axis (azimuthal direction) and ordinary axis (radial direction) of the SWCNTs are labelled. **c**, Polarized Raman spectroscopy where the polarization angle is defined relative to the extraordinary axis of the SWCNTs. The RBM, D and G modes are all labelled. The polarization dependence of the intensity of the G^+ mode gives an angular variation of 7.2°. **d**, Atomic force microscopy map of the surface of the SWCNT film showing the high degree of alignment, a thickness of 3.7 nm and a surface roughness of 1.33 nm.

oblique angles far from normal incidence. Quantum-confined materials such as black phosphorus[8], ReS$_2$ (ref. 9) and one-dimensional crystals[10] all possess in-plane anisotropy. However, only a fraction of these materials have exhibited electrostatic tunability and optical anisotropy[11], and most cannot currently be grown over large areas, which limits their potential to be integrated into electro-optic systems at scale. Because of this, commercial electro-optic systems typically use bulky, anisotropic materials such as LiNbO$_3$, BaTiO$_3$ and CaCO$_3$. Quantum-confined materials, such as one-dimensional single-walled carbon nanotubes (SWCNTs), offer a unique opportunity to replace bulk crystals, enabling integrated, miniaturized and energy-efficient electro-optic systems.

While anisotropy enables polarization-dependent interactions with light, active polarization control requires that the material must also have optical properties that can be tuned using external stimuli such as strain[12], heat[13], electromagnetic fields[14] and electrostatic doping[15]. Electrostatic doping uses an applied voltage to shift the Fermi level, which alters the carrier concentration and optical properties. Electrostatic gating is commonly used in telecommunications systems because of its efficient, fast-switching behaviour and relative ease of fabrication[16]. Although electrostatic doping effects can be observed in Si (ref. 17) and other bulk materials[18,19], the effect is most pronounced in low-dimensional materials. This is because the injected carriers accumulate near the surface of the material, and the optical properties are only tuned in this region.

SWCNTs are one-dimensional, seamless tubes of rolled single-layer graphene. The manner in which the SWCNTs are rolled is described by their chiral indices (n, m), which also determines their band structure. When $(n − m)$ mod $3 ≠ 0$, the SWCNTs are semiconducting[20]; otherwise, they are metallic. The size of the bandgap of semiconducting SWCNTs

is inversely proportional to their diameter. Therefore, through the selection of the chiral indices, the bandgap of SWCNTs can range from 0.1 eV to 1.8 eV (ref. 21). The quantum confinement of carriers into one-dimensional tubes results in SWCNTs having excellent optical and electronic properties[22]. Unaligned systems of SWCNTs have shown tunable optical properties using electrostatic doping[23], and aligned systems of SWCNTs have shown optical anisotropy[24]. Previously, aligned films of unsorted (mixed) metallic and semiconducting SWCNTs have shown tunable optical anisotropy using methods such as chemical doping[25] and ionic liquid gating[26], which are too slow for electro-optical applications where modulation speed is essential such as lidar and free-space optical communication. In addition, these studies focused on either tuning of hyperbolicity in the mid-infrared[25] or tuning the intersub-band plasmon and S$_{22}$ resonances[26] instead of the fundamental S$_{11}$ resonance. Lastly, vacuum filtration is used to fabricate the aligned SWCNT films in previous works, but this process still struggles to produce globally aligned, high-density films at the wafer scale with monolayer thickness[27]. Recent advances in solution-phase separation and assembly approaches have enabled the production of wafer-scale, highly aligned, high-purity semiconducting (99.9999%) SWCNTs[28]. In this paper, we demonstrate giant gate tunability in the optical anisotropy of these SWCNT films. We use spectroscopic ellipsometry to extract the gate-tunable, anisotropic refractive index of the SWCNTs, which is necessary for the future implementation of aligned SWCNTs into electro-optical devices. We also observed that aligned SWCNTs possess the largest normalized birefringence and dichroism in thin films (<4 nm), making them promising candidates to enable active control of light in the visible and near-infrared regimes.
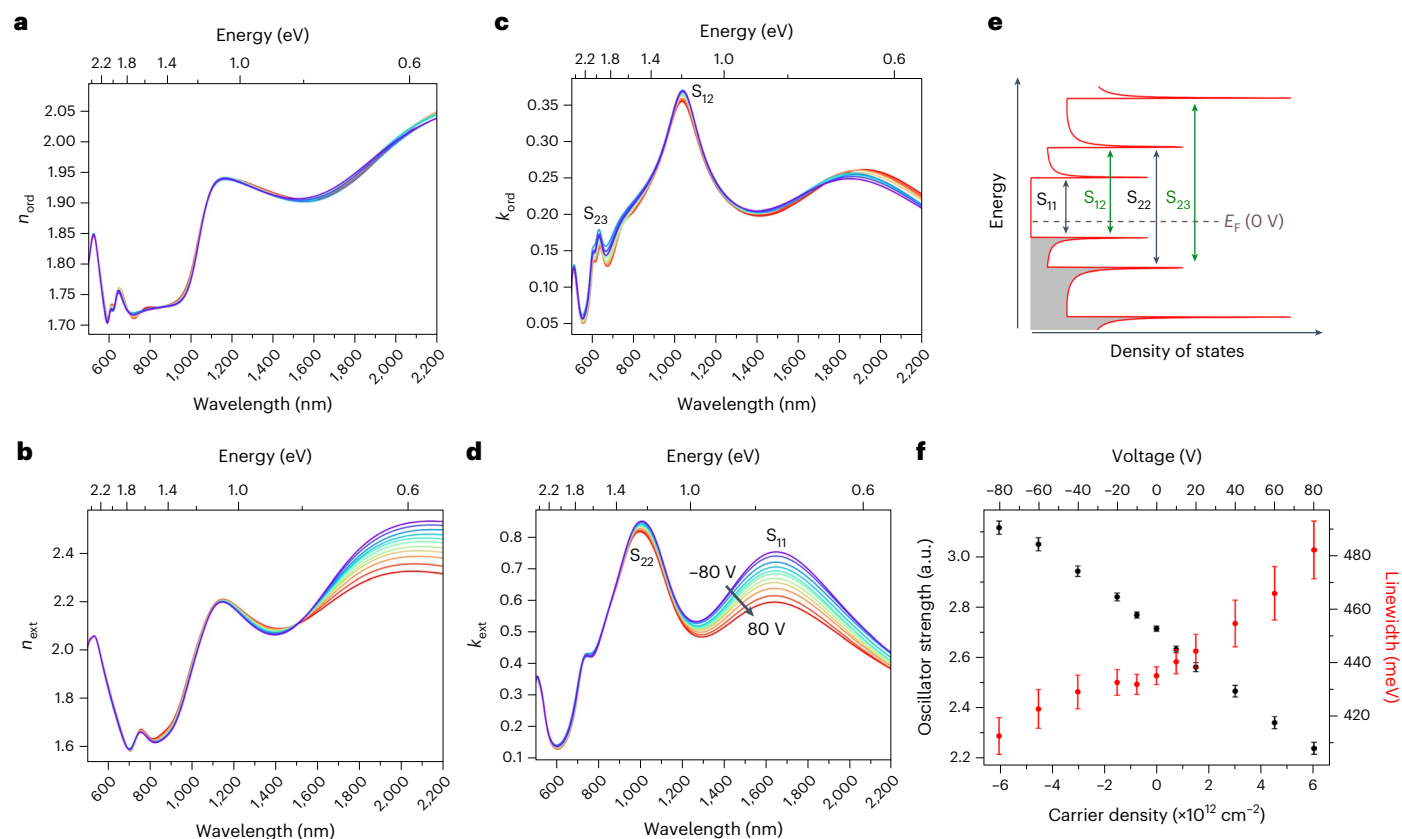
Fig. 2 | Anisotropic, gate-tunable, complex refractive index of SWCNTs.
a,b, The real part of the refractive index along the ordinary (**a**) and extraordinary
(**b**) directions. **c,d**, The imaginary part of the refractive index along the ordinary
(**c**) and extraordinary (**d**) directions with the zero change in angular momentum
transitions (S_{11} and S_{22}) and non-zero change in angular momentum transitions
(S_{12} and S_{23}) labelled. **e**, Schematic of the density of states of semiconducting
SWCNTs with the relevant transitions in the extraordinary (black) and ordinary
(green) directions and Fermi level labelled. Without an applied voltage, the
SWCNTs are naturally p-doped. A positive (negative) applied voltage shifts the
Fermi level to lower (higher) energies. **f**, The gate-tunable oscillator strength and
linewidth of the S_{11} resonance with the fitted uncertainty in the parameters.

We used SWCNTs that were deposited using a multiple dispersion
and sorting process that has been previously reported on to produce
films that are high density and 99.9999% semiconducting[28]. The fabri-
cation process produced 4 inch wafers of globally aligned SWCNT
films, demonstrating that these films can be produced at scale
(Fig. 1a). However, the samples were cut into 1 cm × 1 cm squares for
this study. The top electrical contact is 5 nm of Ti and 45 nm of Au
that was deposited using electron-beam evaporation (Methods) to
make a metal-oxide-semiconductor capacitor (MOSCap) geometry
(Fig. 1b). In the MOSCap geometry, injected charge accumulates near
the SWCNT-dielectric interface, and the charge density drops off
exponentially with a Debye length of ~1 nm (ref. 29). Despite the film
thickness (3.7 nm) being larger than the Debye length, we approxi-
mated the refractive index as being constant throughout the film. The
SWCNT film was grounded while the voltage was applied to the degene-
rately doped Si substrate. Because of this, a positive (negative) voltage
will decrease (increase) the Fermi level, resulting in an increase in the
hole (electron) concentration.

The structural properties of the SWCNTs were studied using
polarization-dependent Raman spectroscopy (Fig. 1c). The radial
breathing modes (RBMs) with Raman shifts between 141 cm^{-1} and
171 cm^{-1} are the result of vibrations along the radial direction of the
nanotubes. The Raman shift of the RBM is determined by the diameter
of the SWCNTs[30] and the width of the RBM indicates the presence of
multiple different diameters within the film. The two most abundant
diameters are 1.46 ± 0.02 nm and 1.57 ± 0.05 nm (see Supplementary
Fig. 1 for additional details). The D-band mode (1,323 cm^{-1}) is caused by

the symmetry-breaking nature of defects within the SWCNTs, showing
that there are some defects present, but its low intensity relative to the
G-band mode indicates a low concentration of defects[31]. The G-band
mode comes from the first-order resonance in bulk graphite samples,
and it redshifts in SWCNTs owing to their curvature and quantum con-
finement effects[32]. The G-band is split into two different modes called
the G$^+$ and G$^-$ modes and the Raman shift difference of these two modes
is consistent with past studies on semiconducting SWCNTs, further
confirming the high quality of the films[32]. The RBM, D and G modes
all disappear in the Raman spectra as the polarization of the incident
light is rotated, which is consistent with all the SWCNTs being aligned
in the same direction. By comparing the intensity of the G$^+$ mode for
light polarized parallel and perpendicular to the extraordinary axis, the
alignment variation of the SWCNTs was calculated to be 7.2° (ref. 28).
Atomic force microscopy further corroborates the highly aligned
nature of the films (Fig. 1c). Using atomic force microscopy, the surface
roughness was calculated to be 1.33 nm, which is much less than both
the spot size (2 mm) and wavelength of light (600–2,200 nm) that was
used for spectroscopic ellipsometry.

The Mueller matrix is a 4 × 4 matrix that relates the Stokes vector
of incident to reflected light, and it comprehensively describes the
polarized light-matter interactions[33]. The normalized Mueller matrix
was measured at 55°, 65° and 75° angles relative to the normal direc-
tion for each voltage with the extraordinary axis of the SWCNTs at
a 40° angle with the in-plane wavevector of the incident light
(Supplementary Fig. 3). The M_{21} element was found to change by up to
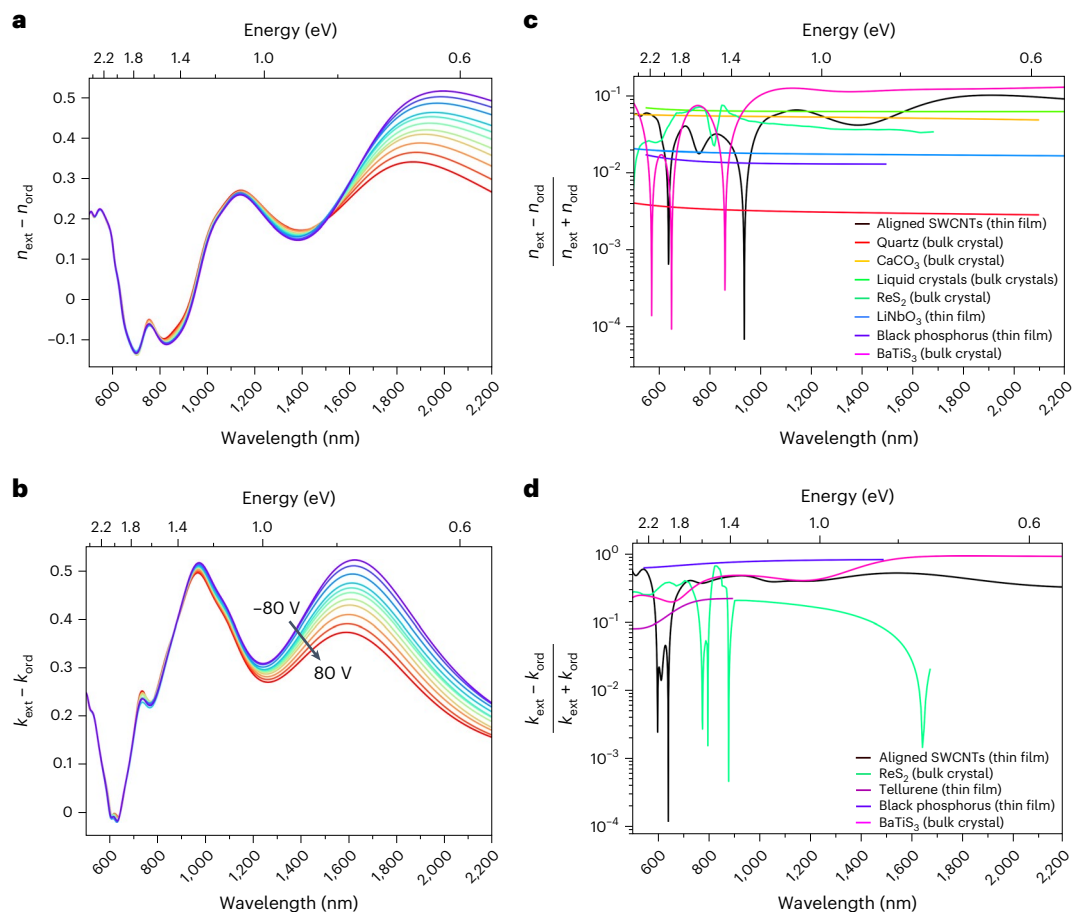0.03, which is much larger than the instrumental uncertainty of ~0.001

Fig. 3 | Gate-tunable, in-plane birefringence and dichroism of SWCNTs.
a,b, The voltage dependence of the birefringence ($n_{ext} - n_{ord}$) (**a**) and dichroism ($k_{ext} - k_{ord}$) (**b**) in highly aligned SWCNTs measured using Mueller matrix ellipsometry. The largest tunability in birefringence and dichroism is observed around the fundamental S_{11} transition. **c,d**, The magnitude of the normalized birefringence ($|n_{ext} - n_{ord}|/(n_{ext} + n_{ord})$) (**c**) and normalized dichroism ($|k_{ext} - k_{ord}|/(k_{ext} + k_{ord})$) (**d**) in highly aligned SWCNTs without an applied voltage is compared with other popular materials with in-plane anisotropy that were measured in either a bulk crystal or thin-film form[10,61–66].

(Supplementary Figs. 4 and 5). In addition, a modulation in normal incidence reflectance was observed in the films using Fourier transform infrared spectroscopy (Supplementary Fig. 7). Therefore, the modulation in the Mueller matrix is due to a change in the refractive index of the SWCNTs instead of random variations between measurements. The anisotropic, complex refractive index was extracted from the Mueller matrix using a multi-Lorentz oscillator model[34] that minimized the root mean squared error (Supplementary Information).

The extracted gate-tunable, complex refractive indices are shown in Fig. 2a–d. The peaks around 1,750 nm and 981 nm in the extraordinary direction are attributed to the S_{11} and S_{22} sub-band excitonic transitions, respectively. The S_{11} peak location differs from the theoretical energies for 1.46 nm and 1.57 nm SWCNTs by 14 meV and 32 meV, respectively[35]. These peaks are broadened since they are the convolution of multiple chiralities of SWCNTs. The two fundamental transitions of S_{12} and S_{23} in the ordinary direction are 1.15 eV and 2.05 eV, respectively. The S_{12} transition is observed near the S_{22} transition (1.19 eV), which is closer than predicted by theory, but it is consistent with previous measurements of the two resonances[36,37]. A peak near the S_{11} transition is also observed in the ordinary direction, but this is attributed to the fact the SWCNTs are not perfectly aligned, allowing ordinarily polarized light to excite the S_{11} transition in some of the nanotubes. The peak in the ordinary direction is redshifted from the extraordinary one to 1,864 nm, which corresponds to an SWCNT diameter of 1.6 nm, which is within the range of diameters observed using polarized Raman spectroscopy. In addition, the same effect is observed by deconvoluting the RBM for various

polarization angles as the intensity of the large-diameter peak is found to be less dependent on the polarization angle than the small-diameter one (Supplementary Fig. 8). This suggests that the larger-diameter SWCNTs do not align as efficiently as smaller ones. The refractive index in the extraordinary direction is found to be larger than in the ordinary direction because optical selection rules require the presence of a phonon for light–matter interactions in the ordinary direction[38]. Not only does the optical selection rule result in the oscillator strength, and refractive index, being largest in the extraordinary direction, but it also results in the extraordinary transitions (S_{11} and S_{22}) being more tunable by injected carriers than the ordinary ones (S_{12} and S_{23})[38]. This observation is consistent with previous measurements on the chemical doping effects of thin films of a mixture of metallic and semiconducting SWCNTs[25]. Wavelengths away from the resonances, such as $\lambda = 850$ nm, were also found to be tunable owing to the broadening and narrowing of the resonant peaks that result in modulation away from the resonant wavelength (Supplementary Fig. 9).

The refractive index can be tuned by injecting charges owing to the plasma dispersion effect (PDE)[39]. The SWCNTs are naturally p-doped owing to ambient adsorbates such as oxygen and water, resulting in the Fermi level being in the lower half of the bandgap[40] (Fig. 2e). When a negative voltage is applied, electrons will be injected into the SWCNTs, making the SWCNT become nearly intrinsic with minimal excess free carriers. The intrinsic nature of the SWCNTs reduces Pauli blocking[41] and increases the oscillator strength[42]. Conversely, when a positive voltage is applied, the SWCNTs become more heavily p-doped,
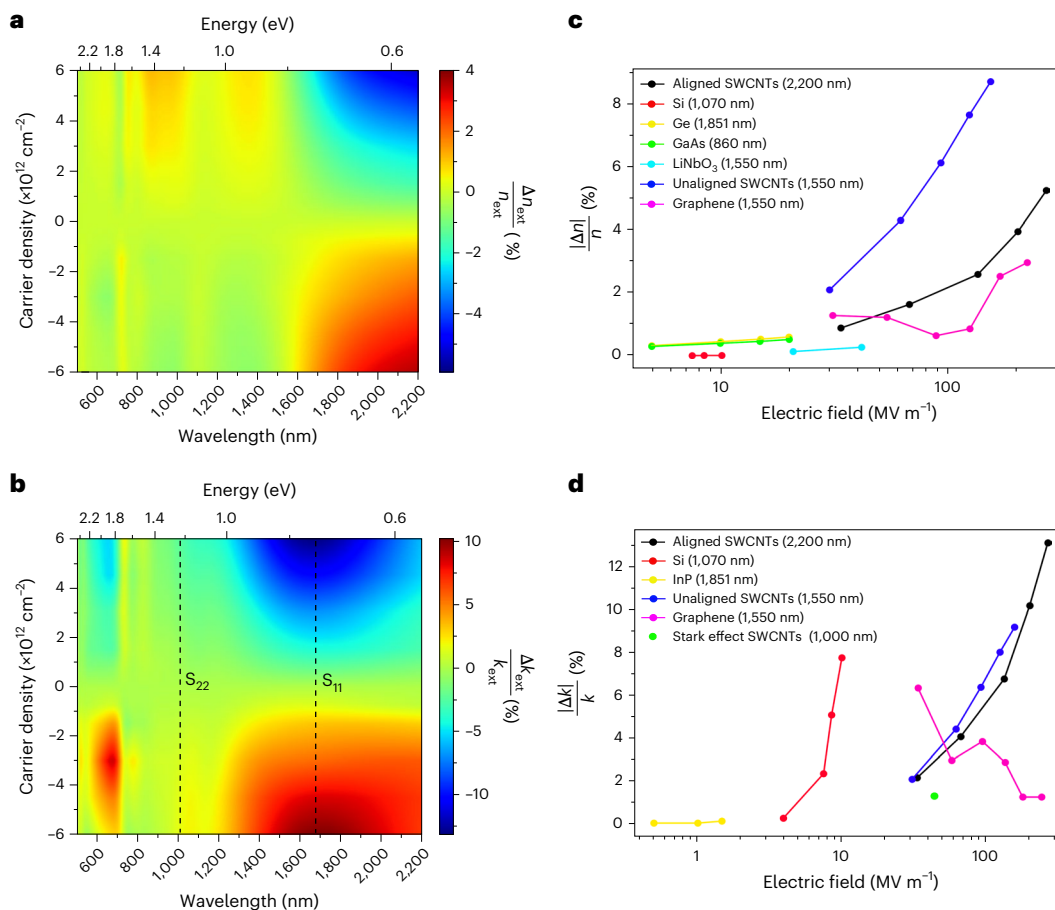
Fig. 4 | Gate tunability of the extraordinary axis of SWCNTs. a,b, The percent change in n (**a**) and k (**b**) of the extraordinary axis of SWCNTs as a function of wavelength and carrier density with the two lowest-order resonances (S_{11} and S_{22}) labelled. **c,d**, Comparison of the tunability in the normalized n (**c**) and normalized k (**d**) of the extraordinary axis of SWCNTs with several other materials commonly used in the infrared regime where the dots represent the data points. The tunability values were taken from the literature[17,19,23,52,67–70].

resulting in increased Pauli blocking and decreased oscillator strength. Therefore, a positive (negative) voltage decreases (increases) the complex refractive index. Although the applied voltage shifts the Fermi level, the voltage is not strong enough to degenerately dope the SWCNTs as seen by the persistence of the S_{11} resonance in k_{ext}. As discussed above, the optical response of excitonic resonances in SWCNTs follows the Lorentz oscillator model with three key parameters for each resonance: the oscillator strength ($f = \frac{N}{2}|\Psi_x(k)|^2$, where N is the carrier density and $\Psi_x(k)$ is the exciton wavefunction in k-space evaluated at the momentum associated with the resonance[43,44]), which is related to the absorptivity of the resonance, the linewidth ($\Gamma = \alpha(m,n)N$, where $\alpha(m,n)$ is the exciton–carrier scattering coefficient that depends on the chirality of the SWCNT[45]) and the resonance energy (E_i)[33]. The gate-dependent oscillator strengths and linewidths of the S_{11} transition are shown in Fig. 2f. The oscillator strength is found to follow the expected linear dependence on carrier concentration, given that the sample is naturally p-doped ($f \propto -N$)[44]. The decrease in oscillator strength suggests that the injected carriers are only ~5% of the amount necessary to fully bleach the S_{11} exciton[46]. The linewidth changes with carrier concentration since an increased number of carriers causes a higher frequency of carrier–carrier scattering events. Therefore, we observe a positive, linear relation between gate voltage and linewidth as predicted previously by theory[45].

The optical anisotropy in SWCNTs is caused by the optical selection rules where an electron can be excited by extraordinarily polarized light without needing a change in its angular momentum, whereas an electron that is excited by ordinarily polarized light must change its angular

momentum. Aligned SWCNTs therefore possess both birefringence ($n_{ext} - n_{ord}$) and dichroism ($k_{ext} - k_{ord}$) because of these optical selection rules (Fig. 3a,b). The depolarization effects of the optical selection rule in the ordinary directions result in dampening of the peaks, which is why the birefringence and dichroism are both positive over the majority of the wavelengths studied. The optical selection rule leads to polarization-dependent optical bandgaps since the fundamental transitions in the extraordinary and ordinary directions are the S_{11} and S_{12} transitions, respectively. Because of this, the normalized dichroism should approach unity for energies between these two transitions. However, the maximum value was only 58% since the SWCNTs are not perfectly aligned. Therefore, dichroism can be further improved by increasing the alignment of SWCNTs. Since the extraordinary refractive index has larger tunability than the ordinary refractive index, the tunability of the birefringence and dichroism is approximately equal to the tunability of the extraordinary refractive index. Therefore, the S_{11} resonance showed the largest tunability for both birefringence and dichroism.

Aligned SWCNTs have normalized birefringence values in the near infrared that are comparable to well-known birefringent materials such as liquid crystals and $CaCO_3$ (Fig. 3c). Aligned SWCNTs also show larger normalized birefringence values than other quantum-confined materials that are gate tunable such as black phosphorus and ReS_2. SWCNTs show larger birefringence than these low-dimensional materials in that the optical selection rules for SWCNTs discussed above result in a relatively large optical bandgap difference between the extraordinary and ordinary axes. The optical bandgap difference for SWCNTs was
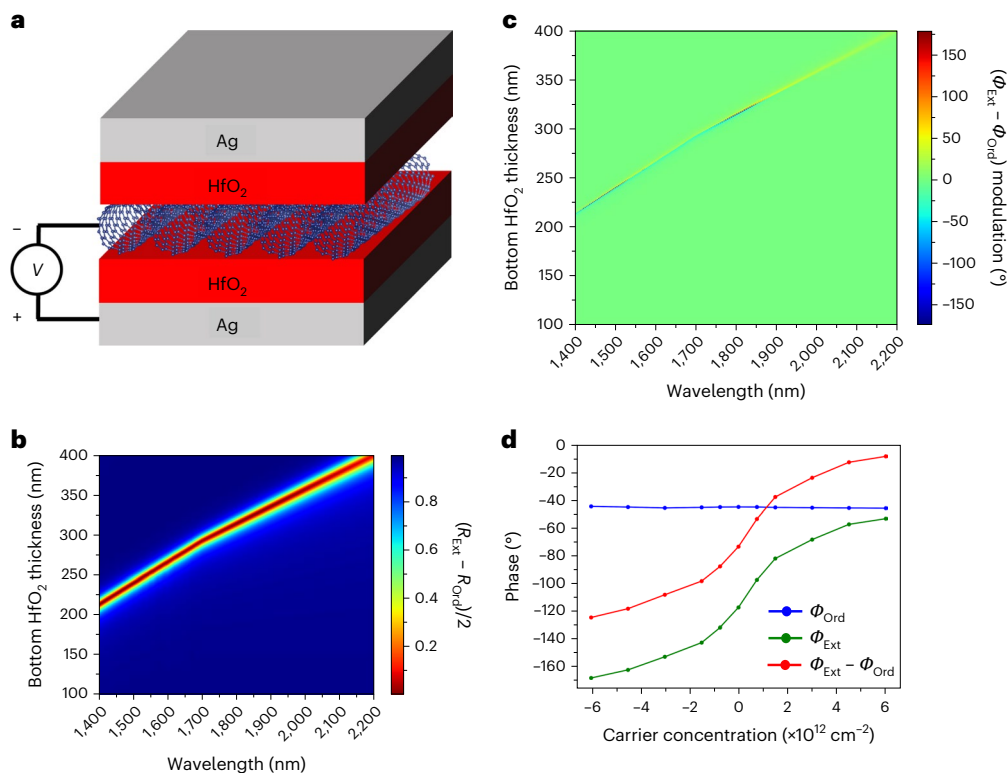
Fig. 5 | Performance of a birefringent phase modulator. a, Design of a closed-cavity phase modulator using highly aligned SWCNTs as the active layer for light at a normal incidence. **b,c**, Average reflectance ($V = 0$ V) (**b**) and phase modulation (**c**) for the modulator with a top Ag thickness of 15 nm and a top HfO$_2$ thickness of 100 nm. These thicknesses were determined by maximizing the phase modulation at $\lambda = 1{,}800$ nm using the transfer matrix method. The modulator was found to have an FoM (FoM = phase modulation/insertion loss) of 15.2°/dB. **d**, Phase of reflected light along the ordinary and extraordinary axes, and their phase difference, for the optimal geometry (the bottom HfO$_2$ thickness is 315 nm) at $\lambda = 1{,}800$ nm for various carrier concentrations within the SWCNT layer.

calculated to be 436 meV, while other low-dimensional materials do not possess similar rules. For example, ReS$_2$ has an optical bandgap difference of 72 meV between its two in-plane, perpendicular axes. Since the optical bandgap difference in SWCNTs is much larger than the linewidth of the S$_{12}$ resonance (210 meV), only the extraordinary direction is excitonic while the ordinary direction acts as a dielectric. To the best of our knowledge, this results in aligned SWCNTs having the largest normalized birefringence of any material <4 nm thick, making it an excellent candidate for compact, energy-efficient, active control of light. Aligned SWCNTs also show a large normalized dichroism value for the same reasons as its large birefringence (Fig. 3d). However, its normalized dichroism is still lower than materials such as BaTiS$_3$ and black phosphorus whose dichroism is the result of crystalline bonds. As discussed above, the aligned SWCNTs normalized dichroism can be further increased by improved fabrication techniques since we still observed some S$_{11}$ absorption in the ordinary direction because the SWCNTs were not perfectly aligned. Further, it should also be noted that black phosphorus and BaTiS$_3$ are only available in bulk single-crystal form where they exhibit this high normalized dichroism, limiting their potential applications. In addition, of all the materials compared, aligned SWCNTs possess the best combination of large, tunable anisotropy with ultrathin, wafer-scale fabrication and ambient environment stability, making it ideal for numerous electro-optical applications.

The normalized change in the real and imaginary parts of the refractive index for various wavelengths and carrier densities (N_c) is shown in Fig. 4a,b, respectively. The carrier density was calculated using a parallel plate capacitor model, $N_c = \frac{\epsilon_0 \epsilon_{SiO2} V_g}{e d_{SiO2}}$, where ϵ_0 is the vacuum permittivity, ϵ_{SiO2} is the relative permittivity of SiO$_2$ (3.9 (ref. 47)), e is the charge of an electron, V_g is the gate voltage and

d_{SiO2} is the thickness of the SiO$_2$ (309 nm). The sign of N_c also indicates that the dominant carrier type where a positive (negative) carrier concentration means that the dominant carrier is holes (electrons). This model assumes that the intrinsic carrier density of the SWCNTs is much less than N_c, which is consistent with SWCNTs of this diameter[48]. Figure 4a,b also uses a two-dimensional interpolation to determine the tunability of the extraordinary refractive index between the carrier densities that were studied. The real and imaginary parts of the refractive index are found to be the most tunable at 2,200 nm and 1,660 nm, respectively. This discrepancy in wavelengths is consistent with the Kramers–Kronig relation where the imaginary part is largest at the resonant wavelength while the real part is largest slightly redshifted from the resonance (Supplementary Fig. 6). The real and imaginary parts of the refractive index show the largest tunability around the S$_{11}$ resonance since it has the largest oscillator strength of all the transitions when $V_g = 0$ V, making it the most susceptible to PDE. The normalized change in the refractive index in the extraordinary direction is compared with other materials in Fig. 4c,d. Bulk semiconductors (Si, Ge and GaAs) all rely on bulk electro-optic effects, such as the Franz–Keldysh and Kerr effects, to tune their refractive index, which enable broadband modulation of their complex refractive indices. However, the magnitude of the change in refractive index is relatively small. Because of the small change in refractive index, electro-optical systems based on these devices require interaction lengths that are typically much longer than the wavelength of light. Unlike these bulk semiconducting materials, the refractive index of SWCNTs, both aligned and unaligned, is dominated by its excitonic transitions. The primary exciton resonance (S$_{11}$) of SWCNTs enables it to achieve larger modulation than traditional bulk semiconductors and III–V multi-quantum wells (Fig. 4c,d). Unaligned SWCNT films are found to have larger modulation

in both n and k than aligned SWCNT films because of the smaller sheet resistances of unaligned films[49,50]. The lower sheet resistance in unaligned films is primarily because unaligned films have more points of contact between nanotubes for charge to transfer. While this lower sheet resistance aids electro-optical tuning, the unaligned tubes do not possess electronic anisotropy and hence do not produce as much birefringence as the aligned nanotubes. In addition, according to the effective medium approximation of a subwavelength grating[51], patterning unaligned SWCNTs does not produce as large of optical anisotropy, and less tunable anisotropy, as the electronic-caused anisotropy of the highly aligned SWCNTs (Supplementary Fig. 10). In addition to the electrostatic-driven PDE that we studied, the S_{11} transition can also be modulated by the Stark effect[52]. However, the Stark effect typically requires an electric field of similar strength to the ones we have studied here to shift the bandgap on the order of several meV without considerably altering the intensity of the peak. Because of this small modulation, its effect is normally only seen at low temperatures, making it unfeasible for large-scale electro-optic applications. In addition, we also found electrostatic gating to yield a larger modulation in SWCNTs than the Stark effect as the imaginary part of the refractive index was modulated by 4.3% from electrostatic gating while it was only modulated by 1.2% by the Stark effect with an equivalent electric field intensity. However, it is worth noting that the Stark effect was measured in semiconducting (6, 5) chirality SWCNTs instead of the 1.46 nm diameter SWCNTs studied here. Therefore, electrostatically doped, highly aligned SWCNTs can achieve larger modulation in its complex refractive index than traditional semiconductors since it is modulating a strong resonance, while electrostatic gating of SWCNTs outperforms the Stark effect in them.

The nanometre-scale thickness of the semiconducting SWCNTs makes it an excellent candidate for low-loss application, which is supported by the observation that it absorbs less light than monolayer graphene (Supplementary Fig. 11). As such, we have designed and simulated a simple, birefringent phase modulator using highly aligned SWCNTs to demonstrate their potential application (Fig. 5a). The SWCNTs are placed between stacks of HfO_2 and Ag to form a high-Q, closed-cavity system. HfO_2 is chosen as the dielectric because it is approximately impedance matched to the ordinary direction of the SWCNTs in the near infrared, which maximizes the anisotropy at the SWCNT–dielectric interface in addition to the ease of conformal thin-film deposition via atomic layer deposition techniques. Likewise, Ag is chosen for the reflective layers owing to its ability to minimize the loss in the system compared with other metals. The reflective nature of the Ag layers forms a high-Q Fabry–Perot cavity that strongly confines light in the HfO_2 and SWCNT layers. The amplitude and phase of reflected light at a normal incidence is simulated using the transfer matrix method[53]. By varying the thicknesses of the two HfO_2 layers, the cavities resonant energy is tuned from $\lambda = 1,400$ nm to 2,200 nm as shown by the reflectance minimum in Fig. 5b. The Fabry–Perot mode is not perfectly linear in Fig. 5b because the real part of the refractive index of the SWCNTs is wavelength dependent. Further information on the absorptance of these modes can be found in Supplementary Fig. 12. The cavity mode also corresponds to the predicted relative phase modulation, which confirms that the phase modulation is caused by a change in the Fabry–Perot cavity by injecting carriers into the SWCNT layer (Fig. 5c). At the near-infrared wavelength of 1,800 nm, the relative phase difference is found to be tuned by −117° (Fig. 5d). The performance of phase modulators is typically quantified using a simple figure of merit (FoM = phase modulation (°)/insertion loss (dB))[54]. Our structure achieves an FoM of 15.2°/dB, which is comparable to phase modulators that use an active layer coupled to a cavity mode with a similar Q-factor[55–59] (Supplementary Table 1). However, the FoM can be increased to the order of 100's by coupling the active material to a cavity mode with an extremely high Q-factor showing an obvious path forward to improving on our design[60]. However, these high FoM phase modulators also rely on bulk active materials. Quantum-confined

systems, such as SWCNTs, have the potential to greatly reduce the energy needed for phase modulation since less material needs to be tuned to observe phase modulation. Nonetheless, as a proof of principle, aligned SWCNTs can be used as a free-space birefringent phase modulator.

Discussion

In conclusion, the tunability in the optical anisotropy of wafer-scale, highly aligned, semiconducting SWCNTs was studied using Mueller matrix ellipsometry. Aligned SWCNTs were found to possess birefringence and dichroism comparable to the most widely used anisotropic materials such as $CaCO_3$ and liquid crystals in the near infrared and the normalized birefringence and dichroism in highly aligned SWCNTs had record values for films <4 nm thick. However, unlike these traditional anisotropic materials, aligned SWCNTs were found to be tunable through electrostatic gating, which will enable them to be implemented into active electro-optic systems without the need of it being incorporated into a heterostructure with an actively tunable material. The real and imaginary parts of the refractive index of these SWCNT films are tuned by 5.9% and 14.3% in the infrared at 2,200 nm and 1,660 nm, respectively, which is larger than the tunability of Si, III–V semiconductors and III–V multi-quantum wells. Our results have the potential to form the basis of ultrathin, compact and energy-efficient electro-optical systems for the active control of the polarization of light, which we have demonstrated by simulating a birefringent phase modulator at $\lambda = 1,800$ nm.

Online content

Any methods, additional references, Nature Portfolio reporting summaries, source data, extended data, supplementary information, acknowledgements, peer review information; details of author contributions and competing interests; and statements of data and code availability are available at https://doi.org/10.1038/s41566-024-01504-0.

References

1. Dong, J. & Zhou, H. Polarimeters from bulky optics to integrated optics: a review. *Opt. Commun.* **465**, 125598 (2020).
2. Zhu, S., Chen, X., Liu, X., Zhang, G. & Tian, P. Recent progress in and perspectives of underwater wireless optical communication. *Prog. Quantum Electron.* **73**, 100274 (2020).
3. Wang, C., Zhang, G., Huang, S., Xie, Y. & Yan, H. The optical properties and plasmonics of anisotropic 2D materials. *Adv. Opt. Mater.* **8**, 1900996 (2020).
4. Kats, M. A. et al. Giant birefringence in optical antenna arrays with widely tailorable optical anisotropy. *Proc. Natl Acad. Sci. USA* **109**, 12364–12368 (2012).
5. Liang, W. Y. et al. Optical anisotropy in layer compounds. *J. Phys. C Solid State Phys.* **6**, 551 (1973).
6. Li, J. et al. Anisotropy of excitons in two-dimensional perovskite crystals. *ACS Nano* **14**, 2156–2161 (2020).
7. Pettersson, L. A. A., Ghosh, S. & Inganäs, O. Optical anisotropy in thin films of poly(3,4-ethylenedioxythiophene)–poly(4-styrenesulfonate). *Org. Electron.* **3**, 143–148 (2002).
8. Yang, H. et al. Optical waveplates based on birefringence of anisotropic two-dimensional layered materials. *ACS Photon.* **4**, 3023–3030 (2017).
9. Ho, C. H., Huang, Y. S., Tiong, K. K. & Liao, P. C. In-plane anisotropy of the optical and electrical properties of layered ReS_2 crystals. *J. Phys. Condens. Matter* **11**, 5367 (1999).
10. Niu, S. et al. Giant optical anisotropy in a quasi-one-dimensional crystal. *Nat. Photon.* **12**, 392–396 (2018).
11. Biswas, S., Grajower, M. Y., Watanabe, K., Taniguchi, T. & Atwater, H. A. Broadband electro-optic polarization conversion with atomically thin black phosphorus. *Science* **374**, 448–453 (2021).

12. Naumis, G. G., Barraza-Lopez, S., Oliva-Leyva, M. & Terrones, H. Electronic and optical properties of strained graphene and other strained 2D materials: a review. *Rep. Prog. Phys.* **80**, 096501 (2017).

13. Lewi, T. et al. Thermally reconfigurable meta-optics. *IEEE Photon. J.* https://doi.org/10.1109/JPHOT.2019.2916161 (2019).

14. Perebeinos, V. & Avouris, P. Exciton ionization, Franz–Keldysh, and Stark effects in carbon nanotubes. *Nano Lett.* **7**, 609–613 (2007).

15. Ahn, C. H. et al. Electrostatic modification of novel materials. *Rev. Mod. Phys.* **78**, 1185–1212 (2006).

16. Beck, M. E. & Hersam, M. C. Emerging opportunities for electrostatic control in atomically thin devices. *ACS Nano* **14**, 6498–6518 (2020).

17. Soref, R. A. & Bennett, B. R. Electrooptical effects in silicon. *IEEE J. Quantum Electron.* **23**, 123–129 (1987).

18. Huang, Y.-W. et al. Gate-tunable conducting oxide metasurfaces. *Nano Lett.* **16**, 5319–5325 (2016).

19. Seraphin, B. O. & Bottka, N. Franz–Keldysh effect of the refractive index in semiconductors. *Phys. Rev.* **139**, A560 (1965).

20. Wildöer, J. W. G., Venema, L. C., Rinzler, A. G., Smalley, R. E. & Dekker, C. Electronic structure of atomically resolved carbon nanotubes. *Nature* **391**, 59–62 (1998).

21. Weisman, R. B. & Bachilo, S. M. Dependence of optical transition energies on structure for single-walled carbon nanotubes in aqueous suspension: an empirical Kataura plot. *Nano Lett.* **3**, 1235–1238 (2003).

22. Nanot, S. et al. Optoelectronic properties of single-wall carbon nanotubes. *Adv. Mater.* **24**, 4977–4994 (2012).

23. Song, B. et al. Giant gate-tunability of complex refractive index in semiconducting carbon nanotubes. *ACS Photon.* **7**, 2896–2905 (2020).

24. De Heer, W. A. et al. Aligned carbon nanotube films: production and optical and electronic properties. *Science* **268**, 845–847 (1995).

25. Roberts, J. A. et al. Tunable hyperbolic metamaterials based on self-assembled carbon nanotubes. *Nano Lett.* **19**, 3131–3137 (2019).

26. Yanagi, K. et al. Intersubband plasmons in the quantum limit in gated and aligned carbon nanotubes. *Nat. Commun.* **9**, 1121 (2018).

27. Gao, W. & Kono, J. Science and applications of wafer-scale crystalline carbon nanotube films prepared through controlled vacuum filtration. *R. Soc. Open Sci.* https://doi.org/10.1098/RSOS.181605 (2019).

28. Liu, L. et al. Aligned, high-density semiconducting carbon nanotube arrays for high-performance electronics. *Science* **368**, 850–856 (2020).

29. Auth, C. P. & Plummer, J. D. Scaling theory for cylindrical, fully-depleted, surrounding-gate MOSFET's. *IEEE Electron Device Lett.* **18**, 74–76 (1997).

30. Bachilo, S. M. et al. Structure-assigned optical spectra of single-walled carbon nanotubes. *Science* **298**, 2361–2366 (2002).

31. Brown, S. D. M., Dresselhaus, M. S., Jorio, A. & Dresselhaus, G. Observations of the *D*-band feature in the Raman spectra of carbon nanotubes. *Phys. Rev. B* **64**, 073403 (2001).

32. Jorio, A. et al. G-Band resonant Raman study of 62 isolated single-wall carbon nanotubes. *Phys. Rev. B* **65**, 155412 (2002).

33. Fujiwara, H. *Spectroscopic Ellipsometry: Principles and Applications* (John Wiley & Sons, 2007).

34. Levi, A. F. J. *Essential Classical Mechanics for Device Physics* (Morgan & Claypool Publishers, 2016).

35. Pedersen, T. G. Exciton effects in carbon nanotubes. *Carbon* **42**, 1007–1010 (2004).

36. Miyauchi, Y., Oba, M. & Maruyama, S. Cross-polarized optical absorption of single-walled nanotubes by polarized photoluminescence excitation spectroscopy. *Phys. Rev. B* **74**, 205440 (2006).

37. Takase, M. et al. Selection-rule breakdown in plasmon-induced electronic excitation of an isolated single-walled carbon nanotube. *Nat. Photon.* **7**, 550–554 (2013).

38. Uryu, S. & Ando, T. Exciton absorption of perpendicularly polarized light in carbon nanotubes. *Phys. Rev. B* **74**, 155411 (2006).

39. Pavesi, L. & Lockwood, D. J. *Silicon Fundamentals for Photonics Applications* (Springer, 2004).

40. Kong, J. et al. Nanotube molecular wires as chemical sensors. *Science* **287**, 622–625 (2000).

41. Sherrott, M. C. et al. Anisotropic quantum well electro-optics in few-layer black phosphorus. *Nano Lett.* **19**, 269–276 (2019).

42. Wu, Z. et al. Transparent, conductive carbon nanotube films. *Science* **305**, 1273–1276 (2004).

43. Schmitt-Rink, S., Chemla, D. S. & Miller, D. A. B. Theory of transient excitonic optical nonlinearities in semiconductor quantum-well structures. *Phys. Rev. B* **32**, 6601 (1985).

44. Lüer, L. et al. Size and mobility of excitons in (6, 5) carbon nanotubes. *Nat. Phys.* **5**, 54–58 (2008).

45. Konabe, S., Matsuda, K. & Okada, S. Suppression of exciton-electron scattering in doped single-walled carbon nanotubes. *Phys. Rev. Lett.* **109**, 187403 (2012).

46. Eckstein, K. H., Oberndorfer, F., Achsnich, M. M., Schöppler, F. & Hertel, T. Quantifying doping levels in carbon nanotubes by optical spectroscopy. *J. Phys. Chem. C* **123**, 30001–30006 (2019).

47. Gray, P. R., Hurst, P. J., Lewis, S. H. & Meyer, R. G. *Analysis and Design of Ananlog Integrated Circuits* (Wiley, 2009).

48. Marulanda, J. M. & Srivastava, A. Carrier density and effective mass calculations in carbon nanotubes. *Phys. Status Solidi B* **245**, 2558–2562 (2008).

49. Behnam, A., Guo, J. & Ural, A. Effects of nanotube alignment and measurement direction on percolation resistivity in single-walled carbon nanotube films. *J. Appl. Phys.* **102**, 44313 (2007).

50. Rahman, R. & Servati, P. Effects of inter-tube distance and alignment on tunnelling resistance and strain sensitivity of nanotube/polymer composite films. *Nanotechnology* **23**, 055703 (2012).

51. Rytov, S. M. Electromagnetic properties of a finely stratified medium. *Sov. Phys. JETP* **2**, 466–475 (1956).

52. Song, D. et al. Measurement of the optical Stark effect in semiconducting carbon nanotubes. *Appl. Phys. A* **96**, 283–287 (2009).

53. Pettersson, L. A. A., Roman, L. S. & Inganäs, O. Modeling photocurrent action spectra of photovoltaic devices based on organic thin films. *J. Appl. Phys.* **86**, 487–496 (1999).

54. Burdin, F., Iskandar, Z., Podevin, F. & Ferrari, P. Design of compact reflection-type phase shifters with high figure-of-merit. *IEEE Trans. Microw. Theory Tech.* **63**, 1883–1893 (2015).

55. Smolyaninov, A., El Amili, A., Vallini, F., Pappert, S. & Fainman, Y. Programmable plasmonic phase modulation of free-space wavefronts at gigahertz rates. *Nat. Photon.* **13**, 431–435 (2019).

56. Forouzmand, A. et al. Tunable all-dielectric metasurface for phase modulation of the reflected and transmitted light via permittivity tuning of indium tin oxide. *Nanophotonics* **8**, 415–427 (2019).

57. Kafaie Shirmanesh, G., Sokhoyan, R., Pala, R. A. & Atwater, H. A. Dual-gated active metasurface at 1550 nm with wide (>300°) phase tunability. *Nano Lett.* **18**, 2957–2963 (2018).

58. Bennett, B. R. & Soref, R. A. Electro-optic Fabry–Perot pixels for phase-dominant spatial light modulators. *Appl. Opt.* **31**, 675–680 (1992).

59. Basile, F., Bloisi, F., Vicari, L. & Simoni, F. Optical phase shift of polymer-dispersed liquid crystals. *Phys. Rev. E* **48**, 432 (1993).

60. Salary, M. M. & Mosallaei, H. Tunable all-dielectric metasurfaces for phase-only modulation of transmitted light based on quasi-bound states in the continuum. *ACS Photon.* **7**, 1813–1829 (2020).

61. Ghosh, G. Dispersion-equation coefficients for the refractive index and birefringence of calcite and quartz crystals. *Opt. Commun.* **163**, 95–102 (1999).

62. Li, J., Wu, S. T., Brugioni, S., Meucci, R. & Faetti, S. Infrared refractive indices of liquid crystals. *J. Appl. Phys.* **97**, 073501 (2005).

63. Munkhbat, B., Wróbel, P., Antosiewicz, T. J. & Shegai, T. O. Optical constants of several multilayer transition metal dichalcogenides measured by spectroscopic ellipsometry in the 300–1700 nm range: high index, anisotropy, and hyperbolicity. *ACS Photon.* **9**, 2398–2407 (2022).

64. Small, D. L., Zelmon, D. E. & Jundt, D. Infrared corrected Sellmeier coefficients for congruently grown lithium niobate and 5 mol.% magnesium oxide–doped lithium niobate. *JOSA B* **14**, 3319–3322 (1997).

65. Lee, S.-Y. & Yee, K.-J. Black phosphorus phase retarder based on anisotropic refractive index dispersion. *2D Mater.* **9**, 015020 (2021).

66. Guo, Z., Gu, H., Fang, M., Ye, L. & Liu, S. Giant in-plane optical and electronic anisotropy of tellurene: a quantitative exploration. *Nanoscale* **14**, 12238–12246 (2022).

67. Wendland, P. H. & Chester, M. Electric field effects on indirect optical transitions in silicon. *Phys. Rev.* **140**, A1384 (1965).

68. Bennett, B. R. & Soref, R. A. Analysis of Franz–Keldysh electro-optic modulation in InP, GaAs, GaSb, InAs, and InSb. In *Proc. SPIE* 158–168 (1987).

69. Li, Z. Q. et al. Dirac charge dynamics in graphene by infrared spectroscopy. *Nat. Phys.* **4**, 532–535 (2008).

70. Jazbinšek, M. & Zgonik, M. Material tensor parameters of LiNbO$_3$ relevant for electro- and elasto-optics. *Appl. Phys. B* **74**, 407–414 (2002).

Methods

SWCNT film fabrication

The highly aligned SWCNT films were prepared using a previous multiple dispersion and sorting process[28]. The 0.3 cm × 0.3 cm metal contacts were deposited under vacuum (<5 × 10^{-6} Torr) using an E-beam evaporator (Kurt J. Lesker PVD 75). The 5 nm Ti and 45 nm Au were deposited sequentially with a deposition rate of 2 Å s^{-1}, and wires were connected using an Ag paste. The sample was grounded using the Ag paste to connect a wire to the p^{++}-silicon substrate.

Optical characterization. Raman spectroscopy and normal incidence reflectance from 600 nm to 1,050 were performed using a Horiba Scientific confocal microscope (LabRAM HR Evolution). This instrument is equipped with an Olympus objective lens (up to ×100) and three different grating (100, 600 and 1,800)-based spectrometers, which are coupled to a Si focal plane array detector. A continuous-wave excitation source with excitation wavelength at 633 nm was used with the ×100 objective lens at 3.2% laser power, which corresponds to a power of 7 μW. The incident light passed through a linear polarizer before interacting with the sample. Reflectance measurements from 1,600 nm to 2,200 nm were performed on a Fourier transform infrared spectrometer (Bruker Vertex 80v) using a liquid nitrogen-cooled MCT-D316-025 detector with a resolution of 16 cm^{-1}. The microscope objective was removed with an internal aperture of 1.5 mm to minimize the angular spread of the incident light. Data were taken at both polarization states using a ZnSe wiregrid polarizer (Thorlabs WP25H-Z) from −80 V to 80 V (Keithley 230). The data were normalized by the reflection from a silver mirror of similar size to the sample.

Mueller matrix ellipsometry

Spectroscopic ellipsometry was completed using a J.A. Woollam-RC2 ellipsometer in Mueller matrix mode, which covers the visible and infrared wavelength regimes (300–2,500 nm). Analysis of the data used the corresponding CompleteEase software to extract the anisotropic, complex optical constants (using a uniaxial, multi-Lorentz oscillator model) as well as film thickness and roughness. Ellipsometry was also performed on the bare SiO$_2$/Si substrate to improve the accuracy of our results.

Data availability

Select anisotropic refractive index values ($V = 0$ V, −80 V and 80 V) are available in Supplementary Table 2. All other data are available upon request of the corresponding author.

Author contributions

D.J. conceived the idea. J.L., E.S., A.A. and B.S. performed ellipsometry, and J.L. fit the experimental results to extract the refractive index. M.K., C.E.S., C.Y.C. and C.F.L. performed supporting experiments under the supervision of J.R.H., S.V., S.L., H.G. and C.R.K. L.-M.P. provided the aligned films. J.L. and D.J. designed the proposed birefringent phase modulator. J.L. performed the simulations and led the writing of the paper with the helpful discussion of the other authors.

Competing interests

The authors declare no competing interests.

Additional information

Supplementary information The online version contains supplementary material available at https://doi.org/10.1038/s41566-024-01504-0.

Correspondence and requests for materials should be addressed to Deep Jariwala.

Peer review information *Nature Photonics* thanks Manish Chhowalla and the other, anonymous, reviewer(s) for their contribution to the peer review of this work.

Reprints and permissions information is available at www.nature.com/reprints.

nature photonics

Gate-tunable optical anisotropy in wafer-scale, aligned carbon nanotube films

In the format provided by the authors and unedited

Table of Contents

(a)

(b)

Figure S1. Identification of diameters and possible chiralities present in thin film. (a) The Raman spectrum of aligned SWCNTs for light polarized parallel to the extraordinary axis was deconvoluted using a least square fit method to a series of Gaussian curves to identify the most common diameters (d_t). **(b)** The diameter of SWCNTs as a function of the chiral indices (n, m) with the confidence regions of the two strongest RBM modes outlined using dashed lines. In total, 13 different semiconducting chiralities (with n > m) fall within these two ranges.

(a)

(b)
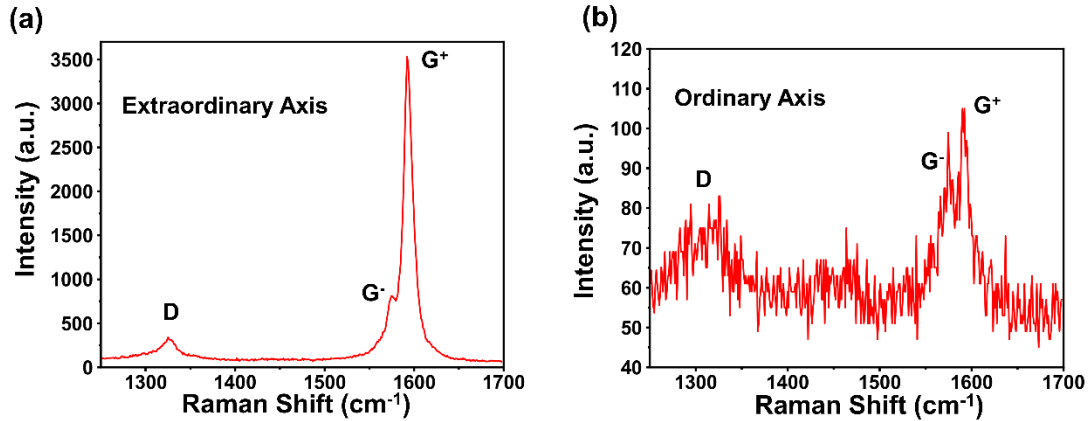
Figure S2. Raman spectra along the principle axes. Polarized Raman spectra for light polarized along the **(a)** extraordinary and **(b)** ordinary directions. The G and D modes are still observed for light polarized along ordinary axis showing the imperfect alignment of the SWCNTs and allowing for the angular variation between nanotubes to be calculated as 7.2°.

Mueller Matrix Ellipsometry

Standard ellipsometry measures the relative amplitude ($\psi = \arctan\left(\frac{|r_{TM}|}{|r_{TE}|}\right)$ where r_{tm} and r_{TE} are the reflection coefficients of the sample for TM and TE polarized light, respectively) and phase ($\Delta = \phi_{TM} - \phi_{TE}$ where ϕ_{TM} and ϕ_{TE} are the phases of TM and TE reflected light, respectively). Since there are two measurements at each wavelength for standard ellipsometry, it can accurately measure both the real and imaginary parts of

the isotropic refractive index. However, for uniaxial, anisotropic materials, a minimum of four measurements at each wavelength is required to determine the complex refractive indices along the ordinary and extraordinary directions. Therefore, standard ellipsometry is insufficient for anisotropic. This lack of information for anisotropic materials can be overcome using multiple measurements of standard ellipsometry where the incident angle of light is varied when the extraordinary axis is out-of-plane, and the sample is rotated around its normal when the extraordinary axis is in-plane. However, a simpler approach for anisotropic materials is to use Mueller matrix ellipsometry.

The normalized Mueller matrix (M) relates the Stokes vector of the incident (S_{inc}) and reflected (S_{ref}) light ($S_{ref} = MS_{inc}$)[1,2]. The Stokes vector completely describes the polarization state of any wave of light, and it is defined as:

$$S = \begin{pmatrix} I_{Total} \\ I_{TM} - I_{TE} \\ I_{45} - I_{-45} \\ I_R - I_L \end{pmatrix} \tag{1}$$

where I is the intensity, and the subscripts describe the polarization (45 and -45 denote the cross polarizations and R and L denote right and left hand circularly polarizations, respectively). The Stokes vector is typically normalized such $I_{Total} = 1$. Since the Stokes vector spans polarization space, the Mueller matrix provides a comprehensive description of the light-matter interactions. Although $M_{11} = 1$ is fixed by the normalization process, Mueller matrix ellipsometry measures the 15 other Mueller matrix elements at every wavelength providing enough information to calculate the complex refractive index of anisotropic measurements.

The complex refractive index ($\tilde{n}$) of a semiconductor is modelled using a series of Lorentz oscillators[3]:

$$\tilde{n}^2(E) = \varepsilon_\infty + \sum_j \frac{f_j \Gamma_j E_j}{E_j^2 - E^2 + i\Gamma_j E_j} \tag{2}$$

where ε_∞ is the static permittivity. The sum is over all of the resonant transitions of the semiconductor. E_j, f_j, and Γ_j are the energy, oscillator strength, and linewidth of the jth resonance, and E is the energy of light. The models refractive index enables the Mueller matrix to be calculated using a transfer matrix method which is fitted to the experimental data by minimizing the root mean-squared error ($RMSE = \sqrt{\frac{1}{15p-q} \sum_i (\psi_i^{Mod} - \psi_i^{Exp})^2 + (\Delta_i^{Mod} - \Delta_i^{Exp})^2}$) where p is the number of wavelengths, q is the number of fit parameters, "Mod" and "Exp" denote the model and experimental values, and the sum is over all of the wavelengths).

In order to ensure the accuracy of our model, we performed Mueller matrix ellipsometry at incident angles of 55°, 65°, and 75°. to reduce the effects of noise. We

also aligned the extraordinary axis of the SWCNTs to a $\approx 35^o$ with the in-plane wavevector of the incident light to observe the effects of the extraordinary and ordinary axes' refractive indices. Standard ellipsometry was also performed on the SiO_2/Si substrate without SWCNTs to determine the thickness of the SiO_2 layer. While fitting the Lorentz oscillator model to the experimental data, we used the CompleteEase software from J.A. Woollam, and the fit parameters were the Lorentz oscillators, the static permittivities, SWCNT layer thickness, and in-plane alignment of the extraordinary axis. The SWCNTs layer thickness and in-plane alignment of the extraordinary axis were determined using the zero voltage measurements, and they were held constant for all other voltages. Our models resulted in RMSE values < 3 which indicates their accuracy.
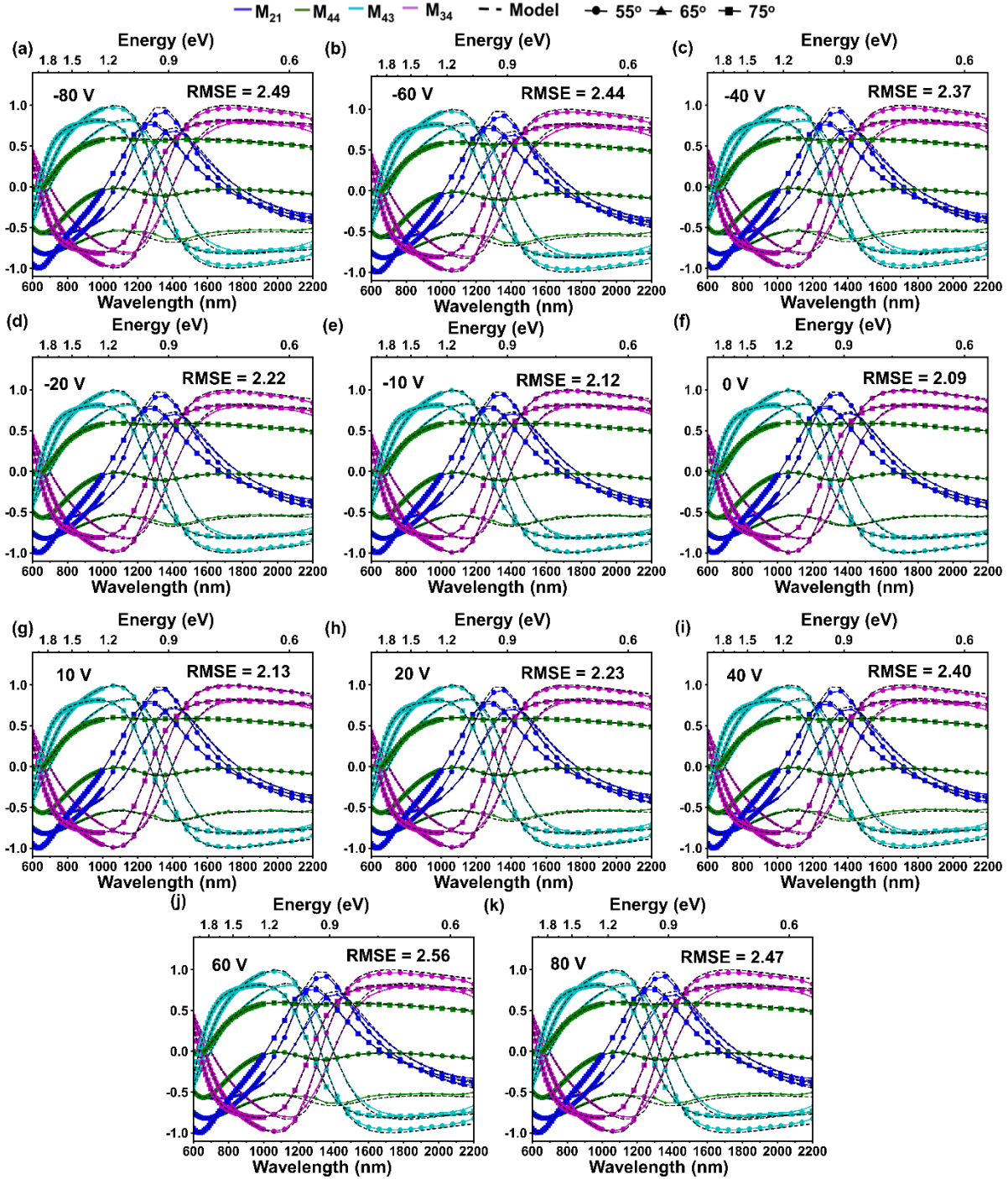
Figure S3. Voltage dependence of select Mueller matrix elements. Experimental and model values of select Mueller matrix elements when the extraordinary axis of the CNTs makes a 40° degree angle with the wavevector of the incident light at voltages of **(a)** -80 V, **(b)** -60 V, **(c)** -40 V, **(d)** -20 V, **(e)** -10 V, **(f)** 0 V, **(g)** 10 V, **(h)** 20 V, **(i)** 40 V, **(j)** 60 V, and **(k)** 80 V with the root-mean-square-error (RMSE) values for each voltage listed.
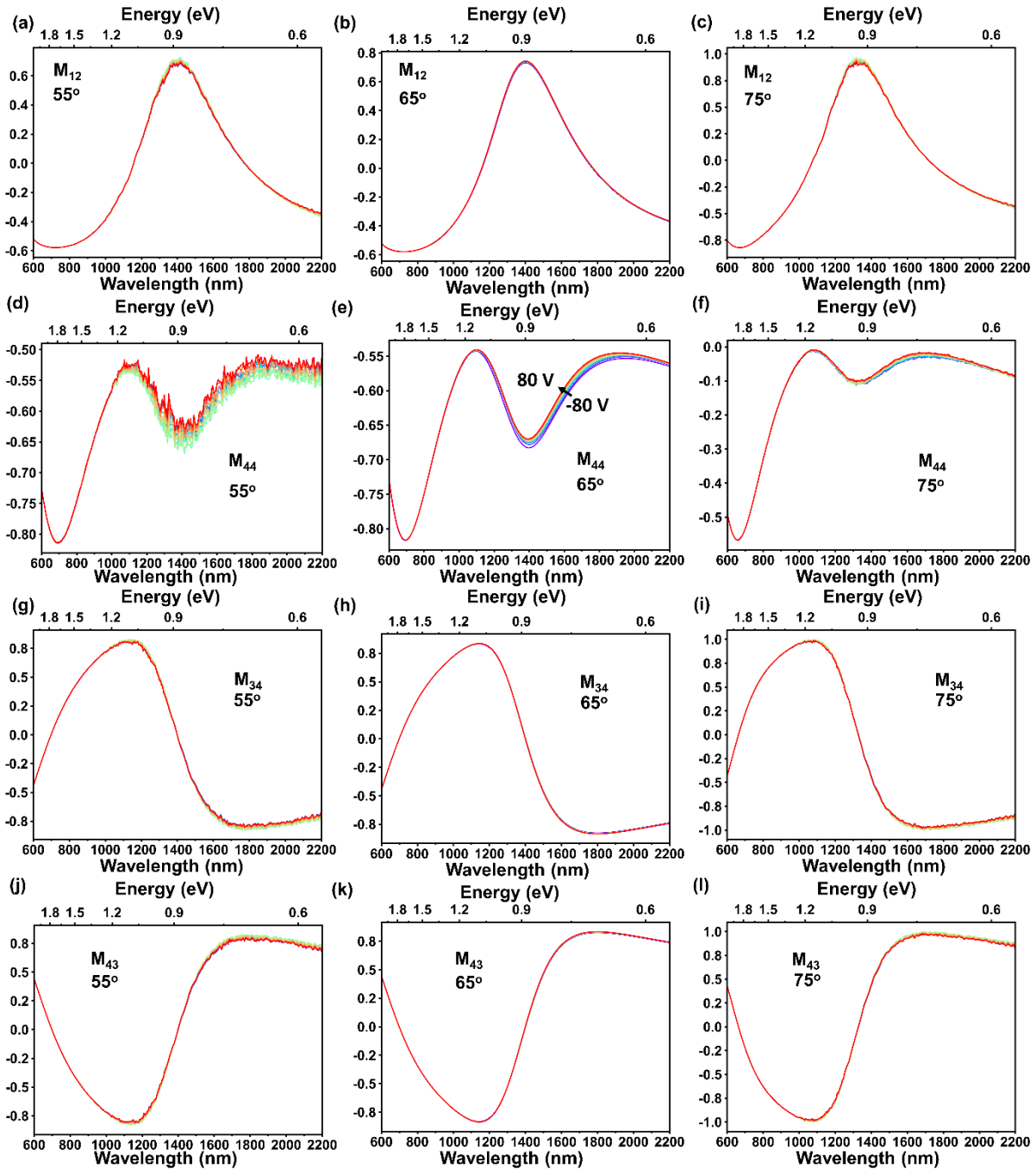
Figure S4. Gate dependence of select Mueller matrix elements. The gate dependence of M_{12} at angles of incidence of **(a)** 55°, **(b)** 65°, and **(c)** 75°, M_{44} at angles of incidence of **(d)** 55°, **(e)** 65°, and **(f)** 75°, M_{34} at angles of incidence of **(g)** 55°, **(h)** 65°, and **(i)** 75°, M_{43} at angles of incidence of **(j)** 55°, **(k)** 65°, and **(l)** 75°.
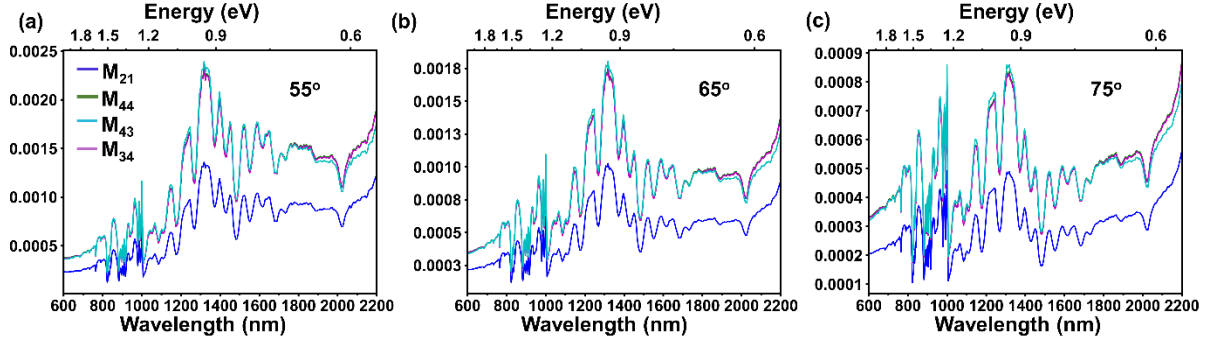
Figure S5. Error of Mueller matrix elements. The uncertainty of select Mueller matrix elements without an applied voltage at incident angles of **(a)** 55°, **(b)** 65°, and **(c)** 75°.
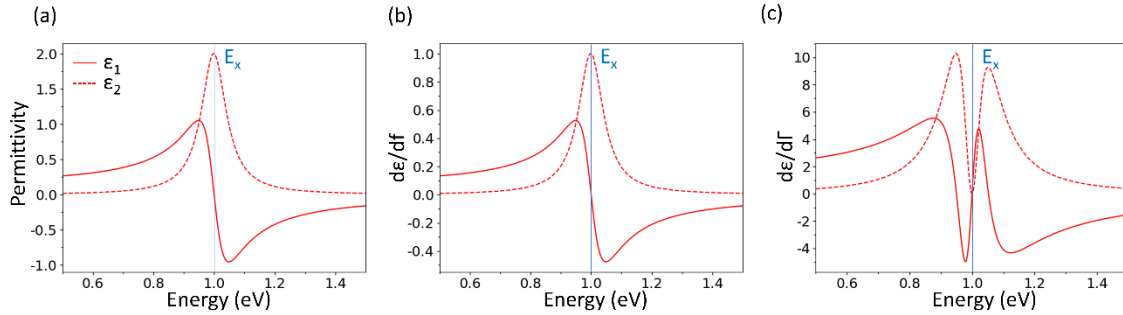
Figure S6. Sensitivity of a Lorentz oscillator. (a) The real (ε_1) and imaginary (ε_2) parts of the permittivity of a Lorentz oscillator calculated using Eq. 2 and $E_x = 1$ eV, $f = 2$, and $\Gamma = 0.1$ eV. The derivative of the permittivity with respect to the **(b)** oscillator strength and **(c)** linewidth of the Lorentz oscillator showing the most sensitive energies of the permittivity to changes in these parameters. While the imaginary part of the permittivity is most sensitive to changes in the oscillator at the resonant energy, the real part is found to be most sensitive at energies below the resonance which is consistent with our findings.
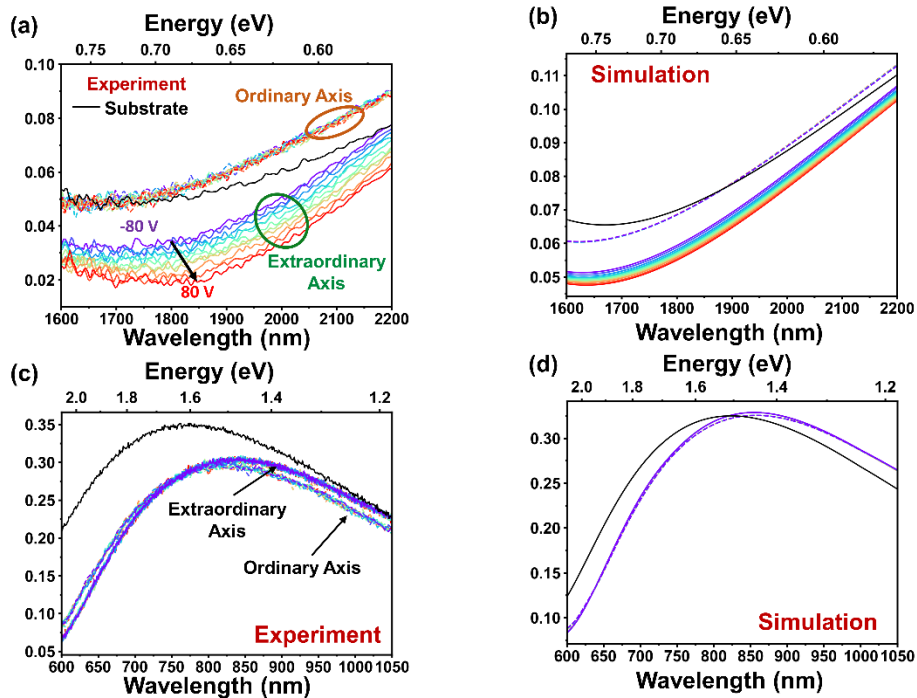
Figure S7. Normal incidence reflectance. (a) Experimental and **(b)** simulated normal incidence reflectance for light polarized along the extraordinary (solid lines) and ordinary (dashed lines) axes as well as the SiO$_2$/Si substrate from λ = 1,600 nm to 2,200 nm. The modulation in reflectance in the extraordinary direction agrees well with those predicted by theory. **(c)** Experimental and **(d)** simulated normal incidence reflectance for light polarized along the extraordinary (solid lines) and ordinary (dashed lines) axes as well as the SiO$_2$/Si substrate from λ = 600 nm to 1,050 nm.
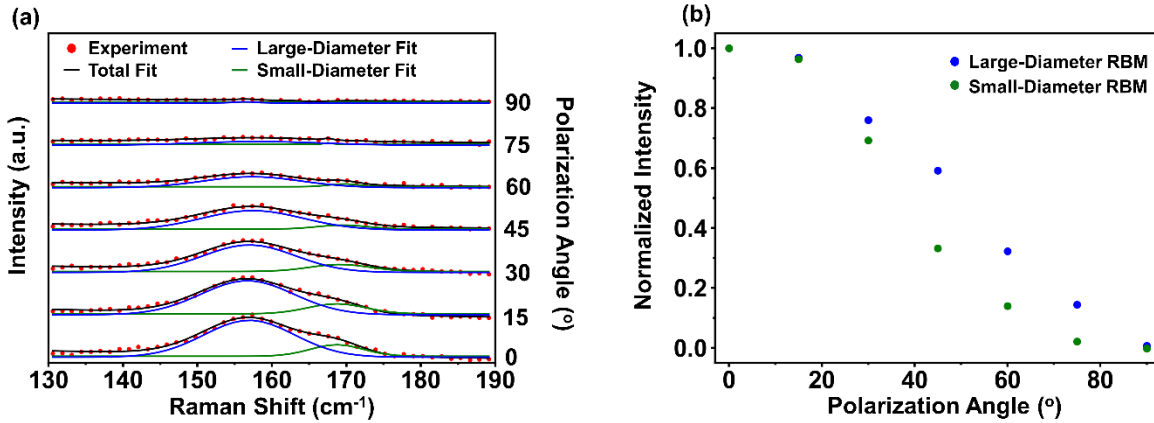
Figure S8. Deconvoluted, polarization-dependent radial breathing mode (RBM). (a) Raman spectra for various incident polarization angles (0° is parallel to the extraordinary axis) of the RBM. The experimental data is fitted to a double Gaussian model with each Gaussian being attributed to relatively large- (smaller Raman shift) and small- (larger Raman shift) diameter SWCNTs. **(b)** The polarization-dependent area-under-the-curve of the two Gaussians normalized to the 0° value. The large-diameter SWCNTs are found to be less dependent on the polarization angle which supports our conclusion that they are less well aligned than the small-diameter SWCNTs. By comparing the intensities at 0° and 90°, the angular variation in alignment is calculated as $\pm 10.4^o$ and $\pm 4.7^o$ for large- and small-diameter SWCNTs, respectively.
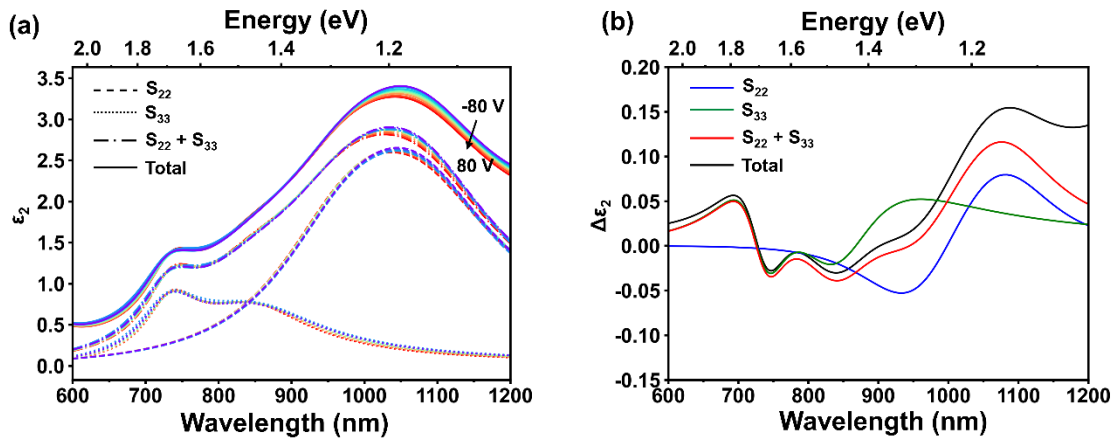
Figure S9. Tunability of optical properties between resonances. (a) Gate-dependent contribution of the S_{22} and S_{33} resonances to the imaginary part of the permittivity (ε_2) of the aligned SWCNTs at and between their resonant energies. **(b)** The gate induced modulation of ε_2 for the S_{22} and S_{33} resonances and the aligned SWCNT film. The total modulation is found to closely follow combined modulation of the S_{22} and S_{33} resonances from 600 to 1050 nm showing that the resonances cause the modulation of the SWCNTs optical properties.
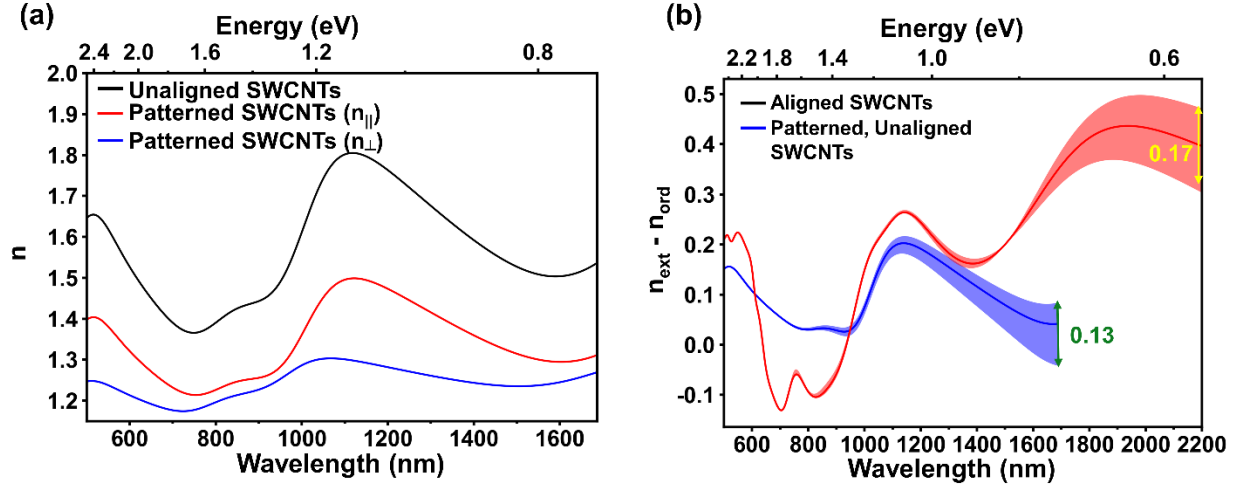
Figure S10. Comparison of aligned SWCNTs and patterned, unaligned SWCNTs using an effective medium approximation. (a) The real part of the refractive index of unaligned SWCNTs and the effective refractive index unaligned SWCNTs patterned into a subwavelength grating[4]. Light polarized parallel (perpendicular) to the repeated unit cell of the grating is denoted by || (⊥). **(b)** The gate-tunable birefringence of the patterned SWCNTs is compared to that of our highly-aligned SWCNTs with the maximum modulations labelled. The shaded region shows the modulation of the two systems for the same maximum applied electric field (± 154 MV/m). The aligned SWCNTs are found to produce larger anisotropy, and that anisotropy is found to be more tunable than patterned SWCNTs.
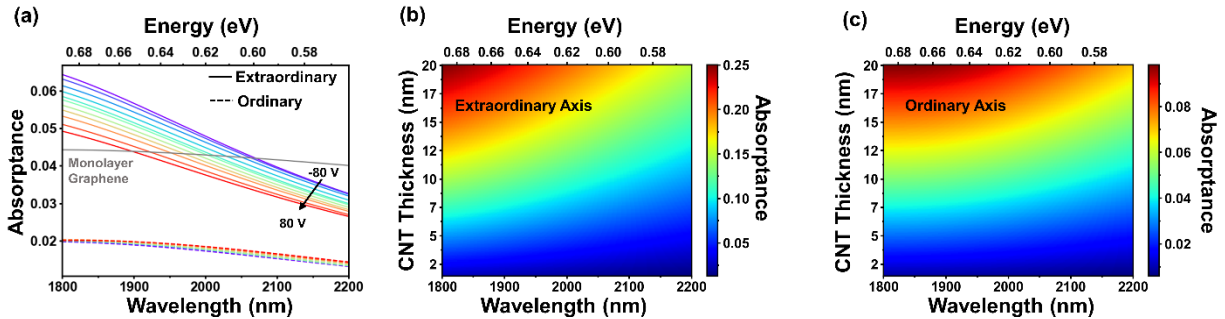
Figure S11. Absorptance of aligned SWCNT films. (a) Gate-dependent absorptance of aligned SWCNTs (3.7 nm) on SiO_2 (309 nm)/Si along the extraordinary (solid lines) and ordinary (dashed) axes. Both directions were found to be less absorptive than monolayer graphene (grey line) for wavelengths longer than 2050 nm. The SWCNT film thickness dependence on an SiO_2/Si substrate along the **(b)** extraordinary and **(c)** ordinary axes.
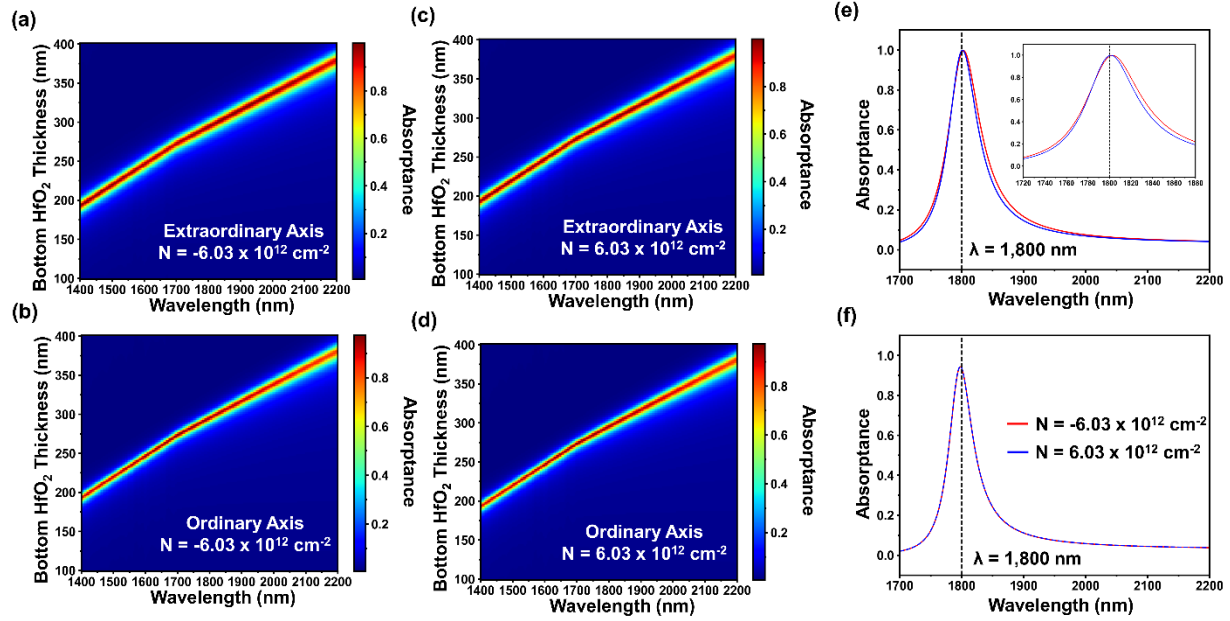
Figure S12. Absorptance of relative phase modulator. Absorptance along the **(a, c)** extraordinary and **(b, d)** ordinary direction of the phase modulator in Figure 5 of the manuscript with $\pm 6.03 \times 10^{12}$ cm^{-2} carriers injected. All of the configurations show an absorptive cavity mode. The absorptance along the **(e)** extraordinary and **(f)** ordinary axes of a device optimized for λ = 1.55 μm in both the on (red) and off (blue) states show that upon the injection of holes, the cavity mode narrows and shifts from 1,800 nm to 1,803 nm in the extraordinary direction causing the phase modulation in that direction. The inset in **(e)** shows the absorption near the resonant wavelength.

Table S1. Performance comparison of several electro-optical phase modulators in the near-infrared.

Active Material (Thickness)	Cavity Mode	Operating Wavelength (nm)	Loss (dB)	Max Phase Modulation (º)	Figure of Merit (º/dB)	Reference
AlN (100 nm)	Plasmonic	1,550	12	180	15	[5]
ITO (5 nm)	Plasmonic Metasurface	1,550	8	303	38	[6]
ITO (3 nm)	Si Nanodisks	1,696	14.2	240	16.9	[7]
AlGaAs/GaAs Multi-Quantum-Well (1,500 nm)	n/a	860	5.7	120	21	[8]
Liquid Crystals	n/a	633	5.2	179	34.4	[9]
LiNbO$_3$ (100 nm)	Notched Silicon (Q > 30,000)	1,564	.409	360	880	[10]
Si (510 nm)	Bound State in the Continuum by patterning Si (Q > 10,000)	1,535	2.3	240	104	[11]
Aligned SWCNTs	Closed Cavity of Ag Mirrors	1,800	7.7	117	15.2	Our Work

Table S2. Anisotropic, complex refractive index of aligned SWCNTs for gate voltages of -80 V, 0 V, and 80 V on an SiO$_2$/Si substrate.

Wavelength (nm)	V = -80 V				V = 0 V				V = 80 V			
	n_{ord}	k_{ord}	n_{ext}	k_{ext}	n_{ord}	k_{ord}	n_{ext}	k_{ext}	n_{ord}	k_{ord}	n_{ext}	k_{ext}
500	1.79	0.10	2.00	0.34	1.80	0.09	2.01	0.34	1.80	0.09	2.01	0.34
501	1.79	0.10	2.00	0.35	1.80	0.09	2.01	0.34	1.80	0.10	2.01	0.34
502	1.80	0.10	2.01	0.35	1.80	0.10	2.01	0.34	1.80	0.10	2.01	0.35
503	1.80	0.11	2.01	0.35	1.80	0.10	2.01	0.35	1.80	0.10	2.01	0.35
504	1.80	0.11	2.01	0.35	1.80	0.10	2.02	0.35	1.80	0.11	2.02	0.35
505	1.80	0.11	2.01	0.36	1.80	0.11	2.02	0.35	1.80	0.11	2.02	0.36
506	1.80	0.11	2.02	0.36	1.80	0.11	2.02	0.36	1.81	0.11	2.02	0.36
507	1.80	0.12	2.02	0.36	1.81	0.11	2.02	0.36	1.81	0.12	2.02	0.36
508	1.81	0.12	2.02	0.36	1.81	0.12	2.03	0.36	1.81	0.12	2.03	0.36
509	1.81	0.12	2.03	0.35	1.81	0.12	2.03	0.36	1.81	0.12	2.03	0.36
510	1.81	0.12	2.03	0.35	1.81	0.12	2.03	0.36	1.81	0.12	2.03	0.36
511	1.81	0.12	2.03	0.35	1.82	0.12	2.03	0.36	1.82	0.12	2.03	0.36
512	1.82	0.12	2.03	0.35	1.82	0.12	2.04	0.35	1.82	0.12	2.04	0.36
513	1.82	0.12	2.04	0.35	1.82	0.12	2.04	0.35	1.82	0.13	2.04	0.35
514	1.82	0.12	2.04	0.34	1.82	0.12	2.04	0.35	1.82	0.13	2.04	0.35
515	1.82	0.12	2.04	0.34	1.83	0.12	2.04	0.35	1.83	0.13	2.04	0.35
516	1.83	0.12	2.04	0.34	1.83	0.12	2.04	0.35	1.83	0.13	2.04	0.35
517	1.83	0.12	2.04	0.34	1.83	0.12	2.05	0.34	1.83	0.13	2.05	0.35
518	1.83	0.12	2.04	0.33	1.83	0.12	2.05	0.34	1.83	0.13	2.05	0.34
519	1.83	0.12	2.04	0.33	1.84	0.12	2.05	0.34	1.84	0.12	2.05	0.34
520	1.84	0.12	2.04	0.33	1.84	0.12	2.05	0.34	1.84	0.12	2.05	0.34
521	1.84	0.11	2.04	0.33	1.84	0.12	2.05	0.33	1.84	0.12	2.05	0.34
522	1.84	0.11	2.05	0.32	1.84	0.12	2.05	0.33	1.84	0.12	2.05	0.33
523	1.84	0.11	2.05	0.32	1.84	0.12	2.05	0.33	1.84	0.12	2.05	0.33
524	1.84	0.11	2.05	0.32	1.84	0.11	2.05	0.32	1.84	0.12	2.05	0.33
525	1.84	0.11	2.05	0.32	1.85	0.11	2.05	0.32	1.85	0.11	2.05	0.32
526	1.84	0.10	2.05	0.31	1.85	0.11	2.05	0.32	1.85	0.11	2.05	0.32
527	1.85	0.10	2.05	0.31	1.85	0.11	2.05	0.32	1.85	0.11	2.05	0.32
528	1.85	0.10	2.05	0.31	1.85	0.10	2.05	0.31	1.85	0.11	2.06	0.31
529	1.85	0.10	2.05	0.31	1.85	0.10	2.05	0.31	1.85	0.10	2.06	0.31
530	1.85	0.09	2.05	0.30	1.85	0.10	2.06	0.31	1.85	0.10	2.06	0.31
531	1.85	0.09	2.05	0.30	1.85	0.10	2.06	0.30	1.85	0.10	2.06	0.30
532	1.85	0.09	2.05	0.30	1.85	0.09	2.06	0.30	1.85	0.09	2.06	0.30
533	1.84	0.09	2.06	0.29	1.85	0.09	2.06	0.30	1.85	0.09	2.06	0.30
534	1.84	0.08	2.06	0.29	1.85	0.09	2.06	0.29	1.85	0.09	2.06	0.29
535	1.84	0.08	2.06	0.28	1.84	0.09	2.06	0.29	1.84	0.09	2.06	0.29
536	1.84	0.08	2.06	0.28	1.84	0.08	2.06	0.28	1.84	0.08	2.06	0.28
537	1.84	0.08	2.06	0.27	1.84	0.08	2.06	0.28	1.84	0.08	2.06	0.28
538	1.84	0.07	2.06	0.27	1.84	0.08	2.06	0.27	1.84	0.08	2.06	0.27

539	1.84	0.07	2.06	0.27	1.84	0.08	2.06	0.27	1.84	0.08	2.06	0.27
540	1.84	0.07	2.06	0.26	1.84	0.07	2.06	0.26	1.84	0.07	2.06	0.26
541	1.83	0.07	2.06	0.26	1.84	0.07	2.06	0.26	1.83	0.07	2.06	0.26
542	1.83	0.07	2.05	0.25	1.83	0.07	2.05	0.26	1.83	0.07	2.05	0.26
543	1.83	0.06	2.05	0.25	1.83	0.07	2.05	0.25	1.83	0.07	2.05	0.25
544	1.83	0.06	2.05	0.24	1.83	0.07	2.05	0.25	1.83	0.07	2.05	0.25
545	1.83	0.06	2.05	0.24	1.83	0.06	2.05	0.24	1.82	0.07	2.05	0.24
546	1.82	0.06	2.05	0.23	1.82	0.06	2.05	0.24	1.82	0.06	2.05	0.24
547	1.82	0.06	2.05	0.23	1.82	0.06	2.04	0.23	1.82	0.06	2.04	0.23
548	1.82	0.06	2.04	0.22	1.82	0.06	2.04	0.23	1.82	0.06	2.04	0.23
549	1.82	0.06	2.04	0.22	1.82	0.06	2.04	0.22	1.81	0.06	2.04	0.22
550	1.81	0.06	2.04	0.21	1.81	0.06	2.04	0.22	1.81	0.06	2.04	0.22
551	1.81	0.05	2.04	0.21	1.81	0.06	2.03	0.22	1.81	0.06	2.03	0.21
552	1.81	0.05	2.03	0.21	1.81	0.06	2.03	0.21	1.81	0.06	2.03	0.21
553	1.81	0.05	2.03	0.20	1.81	0.06	2.03	0.21	1.80	0.06	2.03	0.21
554	1.80	0.05	2.03	0.20	1.80	0.06	2.02	0.20	1.80	0.06	2.02	0.20
555	1.80	0.05	2.02	0.19	1.80	0.06	2.02	0.20	1.80	0.06	2.02	0.20
556	1.80	0.05	2.02	0.19	1.80	0.06	2.02	0.20	1.79	0.06	2.02	0.20
557	1.80	0.05	2.02	0.19	1.79	0.06	2.01	0.19	1.79	0.06	2.01	0.19
558	1.79	0.05	2.01	0.18	1.79	0.06	2.01	0.19	1.79	0.06	2.01	0.19
559	1.79	0.05	2.01	0.18	1.79	0.06	2.01	0.19	1.79	0.06	2.01	0.19
560	1.79	0.05	2.01	0.18	1.79	0.06	2.00	0.18	1.78	0.06	2.00	0.18
561	1.79	0.05	2.00	0.18	1.78	0.06	2.00	0.18	1.78	0.06	2.00	0.18
562	1.78	0.05	2.00	0.17	1.78	0.06	2.00	0.18	1.78	0.06	1.99	0.18
563	1.78	0.05	1.99	0.17	1.78	0.06	1.99	0.18	1.77	0.06	1.99	0.18
564	1.78	0.05	1.99	0.17	1.78	0.06	1.99	0.17	1.77	0.06	1.99	0.17
565	1.78	0.05	1.99	0.17	1.77	0.06	1.99	0.17	1.77	0.06	1.98	0.17
566	1.77	0.05	1.98	0.16	1.77	0.06	1.98	0.17	1.77	0.06	1.98	0.17
567	1.77	0.05	1.98	0.16	1.77	0.06	1.98	0.17	1.76	0.06	1.98	0.17
568	1.77	0.05	1.98	0.16	1.77	0.06	1.97	0.16	1.76	0.06	1.97	0.16
569	1.77	0.05	1.97	0.16	1.76	0.06	1.97	0.16	1.76	0.06	1.97	0.16
570	1.77	0.05	1.97	0.16	1.76	0.06	1.97	0.16	1.76	0.06	1.96	0.16
571	1.76	0.05	1.97	0.15	1.76	0.06	1.96	0.16	1.75	0.06	1.96	0.16
572	1.76	0.06	1.96	0.15	1.76	0.06	1.96	0.16	1.75	0.07	1.96	0.16
573	1.76	0.06	1.96	0.15	1.75	0.06	1.96	0.16	1.75	0.07	1.95	0.16
574	1.76	0.06	1.95	0.15	1.75	0.06	1.95	0.15	1.75	0.07	1.95	0.15
575	1.75	0.06	1.95	0.15	1.75	0.07	1.95	0.15	1.74	0.07	1.94	0.15
576	1.75	0.06	1.95	0.15	1.75	0.07	1.94	0.15	1.74	0.07	1.94	0.15
577	1.75	0.06	1.94	0.14	1.74	0.07	1.94	0.15	1.74	0.07	1.94	0.15
578	1.75	0.06	1.94	0.14	1.74	0.07	1.94	0.15	1.74	0.07	1.93	0.15
579	1.75	0.06	1.94	0.14	1.74	0.07	1.93	0.15	1.73	0.07	1.93	0.15
580	1.74	0.06	1.93	0.14	1.74	0.07	1.93	0.15	1.73	0.08	1.93	0.15
581	1.74	0.07	1.93	0.14	1.73	0.07	1.93	0.15	1.73	0.08	1.92	0.15

582	1.74	0.07	1.93	0.14	1.73	0.08	1.92	0.14	1.73	0.08	1.92	0.15
583	1.74	0.07	1.92	0.14	1.73	0.08	1.92	0.14	1.73	0.08	1.92	0.14
584	1.73	0.07	1.92	0.14	1.73	0.08	1.92	0.14	1.72	0.08	1.91	0.14
585	1.73	0.07	1.91	0.14	1.73	0.08	1.91	0.14	1.72	0.09	1.91	0.14
586	1.73	0.07	1.91	0.14	1.72	0.08	1.91	0.14	1.72	0.09	1.90	0.14
587	1.73	0.07	1.91	0.14	1.72	0.09	1.90	0.14	1.72	0.09	1.90	0.14
588	1.73	0.08	1.90	0.13	1.72	0.09	1.90	0.14	1.72	0.09	1.90	0.14
589	1.72	0.08	1.90	0.13	1.72	0.09	1.90	0.14	1.71	0.10	1.89	0.14
590	1.72	0.08	1.90	0.13	1.72	0.09	1.89	0.14	1.71	0.10	1.89	0.14
591	1.72	0.08	1.89	0.13	1.71	0.10	1.89	0.14	1.71	0.10	1.89	0.14
592	1.72	0.09	1.89	0.13	1.71	0.10	1.89	0.14	1.71	0.10	1.88	0.14
593	1.72	0.09	1.89	0.13	1.71	0.10	1.88	0.14	1.71	0.11	1.88	0.14
594	1.72	0.09	1.88	0.13	1.71	0.10	1.88	0.14	1.71	0.11	1.88	0.14
595	1.71	0.09	1.88	0.13	1.71	0.11	1.88	0.14	1.71	0.11	1.87	0.14
596	1.71	0.10	1.88	0.13	1.71	0.11	1.87	0.14	1.71	0.12	1.87	0.14
597	1.71	0.10	1.87	0.13	1.71	0.11	1.87	0.14	1.71	0.12	1.87	0.14
598	1.71	0.10	1.87	0.13	1.71	0.12	1.87	0.14	1.71	0.13	1.86	0.14
599	1.71	0.11	1.87	0.13	1.71	0.12	1.86	0.14	1.71	0.13	1.86	0.14
600	1.71	0.11	1.86	0.13	1.71	0.13	1.86	0.14	1.71	0.13	1.86	0.14
601	1.71	0.11	1.86	0.13	1.71	0.13	1.86	0.14	1.71	0.13	1.85	0.14
602	1.71	0.12	1.86	0.13	1.71	0.13	1.85	0.14	1.71	0.14	1.85	0.14
603	1.71	0.12	1.85	0.13	1.71	0.13	1.85	0.14	1.71	0.14	1.85	0.14
604	1.71	0.12	1.85	0.13	1.72	0.14	1.85	0.14	1.71	0.14	1.84	0.14
605	1.72	0.13	1.85	0.13	1.72	0.14	1.84	0.14	1.72	0.14	1.84	0.14
606	1.72	0.13	1.85	0.13	1.72	0.14	1.84	0.14	1.72	0.15	1.84	0.14
607	1.72	0.13	1.84	0.13	1.72	0.14	1.84	0.14	1.72	0.15	1.83	0.14
608	1.72	0.13	1.84	0.13	1.72	0.14	1.83	0.14	1.72	0.15	1.83	0.14
609	1.72	0.13	1.84	0.13	1.72	0.14	1.83	0.14	1.72	0.15	1.83	0.14
610	1.73	0.14	1.83	0.13	1.73	0.14	1.83	0.14	1.72	0.15	1.82	0.14
611	1.73	0.14	1.83	0.13	1.73	0.14	1.82	0.14	1.73	0.15	1.82	0.14
612	1.73	0.14	1.83	0.13	1.73	0.14	1.82	0.14	1.73	0.15	1.82	0.14
613	1.73	0.14	1.82	0.13	1.73	0.14	1.82	0.14	1.73	0.15	1.81	0.14
614	1.73	0.14	1.82	0.13	1.73	0.14	1.82	0.14	1.73	0.15	1.81	0.14
615	1.73	0.14	1.82	0.13	1.73	0.14	1.81	0.14	1.73	0.15	1.81	0.14
616	1.73	0.14	1.81	0.13	1.73	0.14	1.81	0.14	1.73	0.15	1.80	0.14
617	1.73	0.14	1.81	0.13	1.73	0.14	1.81	0.14	1.73	0.15	1.80	0.14
618	1.73	0.13	1.81	0.13	1.73	0.14	1.80	0.14	1.73	0.15	1.80	0.14
619	1.73	0.13	1.81	0.13	1.73	0.14	1.80	0.14	1.73	0.15	1.80	0.14
620	1.73	0.13	1.80	0.13	1.73	0.14	1.80	0.14	1.73	0.15	1.79	0.14
621	1.73	0.14	1.80	0.13	1.73	0.14	1.79	0.14	1.73	0.15	1.79	0.14
622	1.73	0.14	1.80	0.13	1.73	0.15	1.79	0.14	1.73	0.15	1.79	0.14
623	1.73	0.14	1.79	0.13	1.73	0.15	1.79	0.14	1.73	0.15	1.78	0.14
624	1.73	0.14	1.79	0.13	1.73	0.15	1.78	0.14	1.73	0.16	1.78	0.14

625	1.73	0.14	1.79	0.14	1.73	0.15	1.78	0.14	1.73	0.16	1.78	0.14
626	1.73	0.14	1.78	0.14	1.73	0.15	1.78	0.14	1.73	0.16	1.77	0.15
627	1.73	0.14	1.78	0.14	1.73	0.15	1.78	0.14	1.73	0.16	1.77	0.15
628	1.73	0.14	1.78	0.14	1.73	0.15	1.77	0.14	1.73	0.16	1.77	0.15
629	1.73	0.14	1.78	0.14	1.73	0.16	1.77	0.15	1.73	0.16	1.77	0.15
630	1.73	0.14	1.77	0.14	1.73	0.16	1.77	0.15	1.73	0.16	1.76	0.15
631	1.73	0.15	1.77	0.14	1.73	0.16	1.76	0.15	1.73	0.17	1.76	0.15
632	1.73	0.15	1.77	0.14	1.73	0.16	1.76	0.15	1.73	0.17	1.76	0.15
633	1.73	0.15	1.76	0.14	1.73	0.16	1.76	0.15	1.73	0.17	1.75	0.15
634	1.74	0.15	1.76	0.14	1.73	0.16	1.75	0.15	1.74	0.17	1.75	0.15
635	1.74	0.15	1.76	0.14	1.74	0.16	1.75	0.15	1.74	0.17	1.75	0.15
636	1.74	0.15	1.75	0.14	1.74	0.17	1.75	0.15	1.74	0.17	1.74	0.15
637	1.74	0.15	1.75	0.14	1.74	0.17	1.75	0.15	1.74	0.17	1.74	0.16
638	1.74	0.15	1.75	0.15	1.74	0.17	1.74	0.15	1.74	0.17	1.74	0.16
639	1.74	0.15	1.75	0.15	1.74	0.17	1.74	0.15	1.75	0.17	1.74	0.16
640	1.74	0.15	1.74	0.15	1.74	0.17	1.74	0.16	1.75	0.17	1.73	0.16
641	1.74	0.16	1.74	0.15	1.75	0.17	1.73	0.16	1.75	0.17	1.73	0.16
642	1.75	0.16	1.74	0.15	1.75	0.17	1.73	0.16	1.75	0.17	1.73	0.16
643	1.75	0.16	1.73	0.15	1.75	0.17	1.73	0.16	1.75	0.17	1.72	0.16
644	1.75	0.16	1.73	0.15	1.75	0.16	1.73	0.16	1.75	0.17	1.72	0.16
645	1.75	0.15	1.73	0.15	1.75	0.16	1.72	0.16	1.75	0.17	1.72	0.16
646	1.75	0.15	1.73	0.15	1.75	0.16	1.72	0.16	1.76	0.16	1.71	0.17
647	1.75	0.15	1.72	0.16	1.75	0.16	1.72	0.16	1.76	0.16	1.71	0.17
648	1.76	0.15	1.72	0.16	1.76	0.16	1.71	0.17	1.76	0.16	1.71	0.17
649	1.76	0.15	1.72	0.16	1.76	0.16	1.71	0.17	1.76	0.16	1.71	0.17
650	1.76	0.15	1.71	0.16	1.76	0.16	1.71	0.17	1.76	0.16	1.70	0.17
651	1.76	0.15	1.71	0.16	1.76	0.16	1.71	0.17	1.76	0.16	1.70	0.17
652	1.76	0.15	1.71	0.16	1.76	0.15	1.70	0.17	1.76	0.16	1.70	0.17
653	1.76	0.15	1.70	0.16	1.76	0.15	1.70	0.17	1.76	0.15	1.69	0.18
654	1.76	0.15	1.70	0.17	1.76	0.15	1.70	0.17	1.76	0.15	1.69	0.18
655	1.76	0.15	1.70	0.17	1.76	0.15	1.69	0.18	1.76	0.15	1.69	0.18
656	1.76	0.14	1.70	0.17	1.76	0.15	1.69	0.18	1.76	0.15	1.69	0.18
657	1.76	0.14	1.69	0.17	1.76	0.15	1.69	0.18	1.76	0.15	1.68	0.18
658	1.76	0.14	1.69	0.17	1.76	0.15	1.69	0.18	1.75	0.15	1.68	0.19
659	1.76	0.14	1.69	0.17	1.76	0.15	1.68	0.18	1.75	0.15	1.68	0.19
660	1.76	0.14	1.68	0.17	1.75	0.15	1.68	0.18	1.75	0.15	1.67	0.19
661	1.76	0.14	1.68	0.18	1.75	0.15	1.68	0.19	1.75	0.15	1.67	0.19
662	1.76	0.14	1.68	0.18	1.75	0.14	1.67	0.19	1.75	0.15	1.67	0.19
663	1.76	0.14	1.68	0.18	1.75	0.14	1.67	0.19	1.75	0.15	1.67	0.20
664	1.76	0.14	1.67	0.18	1.75	0.14	1.67	0.19	1.75	0.15	1.66	0.20
665	1.76	0.13	1.67	0.18	1.75	0.14	1.67	0.19	1.75	0.15	1.66	0.20
666	1.76	0.13	1.67	0.19	1.75	0.14	1.66	0.20	1.75	0.14	1.66	0.20
667	1.76	0.13	1.66	0.19	1.75	0.14	1.66	0.20	1.75	0.14	1.66	0.20

668	1.75	0.13	1.66	0.19	1.75	0.14	1.66	0.20	1.75	0.14	1.65	0.21
669	1.75	0.13	1.66	0.19	1.75	0.14	1.65	0.20	1.74	0.14	1.65	0.21
670	1.75	0.13	1.66	0.20	1.75	0.14	1.65	0.21	1.74	0.14	1.65	0.21
671	1.75	0.13	1.65	0.20	1.74	0.14	1.65	0.21	1.74	0.14	1.64	0.21
672	1.75	0.13	1.65	0.20	1.74	0.14	1.65	0.21	1.74	0.14	1.64	0.22
673	1.75	0.13	1.65	0.20	1.74	0.14	1.64	0.21	1.74	0.14	1.64	0.22
674	1.75	0.13	1.64	0.21	1.74	0.14	1.64	0.22	1.74	0.14	1.64	0.22
675	1.75	0.13	1.64	0.21	1.74	0.14	1.64	0.22	1.74	0.14	1.63	0.22
676	1.75	0.13	1.64	0.21	1.74	0.14	1.64	0.22	1.74	0.14	1.63	0.23
677	1.74	0.13	1.64	0.21	1.74	0.14	1.63	0.22	1.74	0.15	1.63	0.23
678	1.74	0.13	1.63	0.22	1.74	0.14	1.63	0.23	1.74	0.15	1.63	0.23
679	1.74	0.13	1.63	0.22	1.74	0.14	1.63	0.23	1.74	0.15	1.63	0.24
680	1.74	0.13	1.63	0.22	1.74	0.14	1.63	0.23	1.73	0.15	1.62	0.24
681	1.74	0.13	1.63	0.22	1.74	0.14	1.62	0.24	1.73	0.15	1.62	0.24
682	1.74	0.13	1.62	0.23	1.73	0.14	1.62	0.24	1.73	0.15	1.62	0.25
683	1.74	0.13	1.62	0.23	1.73	0.14	1.62	0.24	1.73	0.15	1.62	0.25
684	1.74	0.13	1.62	0.23	1.73	0.14	1.62	0.25	1.73	0.15	1.61	0.25
685	1.74	0.13	1.62	0.24	1.73	0.15	1.62	0.25	1.73	0.15	1.61	0.26
686	1.74	0.13	1.61	0.24	1.73	0.15	1.61	0.25	1.73	0.15	1.61	0.26
687	1.73	0.13	1.61	0.24	1.73	0.15	1.61	0.26	1.73	0.15	1.61	0.26
688	1.73	0.13	1.61	0.25	1.73	0.15	1.61	0.26	1.73	0.15	1.61	0.27
689	1.73	0.13	1.61	0.25	1.73	0.15	1.61	0.26	1.73	0.15	1.60	0.27
690	1.73	0.13	1.61	0.26	1.73	0.15	1.61	0.27	1.73	0.15	1.60	0.27
691	1.73	0.13	1.60	0.26	1.73	0.15	1.60	0.27	1.73	0.15	1.60	0.28
692	1.73	0.13	1.60	0.26	1.73	0.15	1.60	0.27	1.73	0.15	1.60	0.28
693	1.73	0.13	1.60	0.27	1.73	0.15	1.60	0.28	1.72	0.15	1.60	0.28
694	1.73	0.13	1.60	0.27	1.73	0.15	1.60	0.28	1.72	0.15	1.60	0.29
695	1.73	0.14	1.60	0.27	1.73	0.15	1.60	0.28	1.72	0.16	1.60	0.29
696	1.73	0.14	1.59	0.28	1.72	0.15	1.60	0.29	1.72	0.16	1.59	0.30
697	1.72	0.14	1.59	0.28	1.72	0.15	1.60	0.29	1.72	0.16	1.59	0.30
698	1.72	0.14	1.59	0.29	1.72	0.15	1.59	0.30	1.72	0.16	1.59	0.30
699	1.72	0.14	1.59	0.29	1.72	0.15	1.59	0.30	1.72	0.16	1.59	0.31
700	1.72	0.14	1.59	0.30	1.72	0.16	1.59	0.30	1.72	0.16	1.59	0.31
701	1.72	0.14	1.59	0.30	1.72	0.16	1.59	0.31	1.72	0.16	1.59	0.32
702	1.72	0.14	1.59	0.30	1.72	0.16	1.59	0.31	1.72	0.16	1.59	0.32
703	1.72	0.14	1.59	0.31	1.72	0.16	1.59	0.32	1.72	0.16	1.59	0.32
704	1.72	0.14	1.59	0.31	1.72	0.16	1.59	0.32	1.72	0.16	1.59	0.33
705	1.72	0.14	1.58	0.32	1.72	0.16	1.59	0.32	1.72	0.16	1.59	0.33
706	1.72	0.14	1.58	0.32	1.72	0.16	1.59	0.33	1.72	0.16	1.59	0.34
707	1.72	0.15	1.58	0.33	1.72	0.16	1.59	0.33	1.72	0.16	1.59	0.34
708	1.72	0.15	1.58	0.33	1.72	0.16	1.59	0.34	1.72	0.17	1.59	0.35
709	1.72	0.15	1.58	0.34	1.72	0.16	1.59	0.34	1.72	0.17	1.59	0.35
710	1.72	0.15	1.58	0.34	1.72	0.16	1.59	0.35	1.72	0.17	1.59	0.35

711	1.72	0.15	1.58	0.35	1.72	0.16	1.59	0.35	1.72	0.17	1.59	0.36
712	1.72	0.15	1.59	0.35	1.72	0.16	1.59	0.35	1.72	0.17	1.59	0.36
713	1.71	0.15	1.59	0.36	1.72	0.17	1.59	0.36	1.72	0.17	1.59	0.37
714	1.71	0.15	1.59	0.36	1.72	0.17	1.59	0.36	1.72	0.17	1.60	0.37
715	1.71	0.15	1.59	0.36	1.72	0.17	1.59	0.37	1.72	0.17	1.60	0.37
716	1.71	0.15	1.59	0.37	1.72	0.17	1.60	0.37	1.72	0.17	1.60	0.38
717	1.71	0.16	1.59	0.37	1.72	0.17	1.60	0.37	1.72	0.17	1.60	0.38
718	1.71	0.16	1.59	0.38	1.72	0.17	1.60	0.38	1.72	0.17	1.60	0.38
719	1.71	0.16	1.59	0.38	1.72	0.17	1.60	0.38	1.72	0.17	1.60	0.39
720	1.71	0.16	1.60	0.39	1.72	0.17	1.60	0.38	1.72	0.17	1.61	0.39
721	1.71	0.16	1.60	0.39	1.72	0.17	1.60	0.39	1.72	0.18	1.61	0.39
722	1.71	0.16	1.60	0.39	1.72	0.17	1.61	0.39	1.72	0.18	1.61	0.40
723	1.71	0.16	1.60	0.40	1.72	0.17	1.61	0.39	1.72	0.18	1.61	0.40
724	1.71	0.16	1.60	0.40	1.72	0.17	1.61	0.40	1.72	0.18	1.61	0.40
725	1.71	0.16	1.61	0.40	1.72	0.17	1.61	0.40	1.72	0.18	1.62	0.40
726	1.71	0.17	1.61	0.41	1.72	0.18	1.61	0.40	1.72	0.18	1.62	0.41
727	1.71	0.17	1.61	0.41	1.72	0.18	1.62	0.40	1.72	0.18	1.62	0.41
728	1.71	0.17	1.62	0.41	1.72	0.18	1.62	0.41	1.72	0.18	1.62	0.41
729	1.71	0.17	1.62	0.41	1.72	0.18	1.62	0.41	1.72	0.18	1.62	0.41
730	1.71	0.17	1.62	0.42	1.72	0.18	1.62	0.41	1.72	0.18	1.63	0.41
731	1.71	0.17	1.62	0.42	1.72	0.18	1.62	0.41	1.72	0.18	1.63	0.42
732	1.71	0.17	1.63	0.42	1.72	0.18	1.63	0.41	1.72	0.18	1.63	0.42
733	1.71	0.17	1.63	0.42	1.72	0.18	1.63	0.42	1.72	0.18	1.63	0.42
734	1.71	0.17	1.63	0.42	1.72	0.18	1.63	0.42	1.72	0.18	1.64	0.42
735	1.71	0.17	1.64	0.43	1.72	0.18	1.63	0.42	1.72	0.18	1.64	0.42
736	1.71	0.18	1.64	0.43	1.72	0.18	1.64	0.42	1.72	0.19	1.64	0.42
737	1.71	0.18	1.64	0.43	1.72	0.18	1.64	0.42	1.72	0.19	1.64	0.42
738	1.71	0.18	1.64	0.43	1.72	0.18	1.64	0.42	1.72	0.19	1.64	0.42
739	1.71	0.18	1.65	0.43	1.72	0.18	1.64	0.42	1.72	0.19	1.65	0.42
740	1.71	0.18	1.65	0.43	1.72	0.18	1.64	0.42	1.72	0.19	1.65	0.42
741	1.71	0.18	1.65	0.43	1.72	0.18	1.65	0.42	1.72	0.19	1.65	0.42
742	1.71	0.18	1.65	0.43	1.72	0.19	1.65	0.42	1.72	0.19	1.65	0.42
743	1.72	0.18	1.66	0.43	1.72	0.19	1.65	0.42	1.72	0.19	1.65	0.42
744	1.72	0.18	1.66	0.43	1.72	0.19	1.65	0.42	1.72	0.19	1.65	0.42
745	1.72	0.18	1.66	0.43	1.72	0.19	1.65	0.43	1.72	0.19	1.66	0.42
746	1.72	0.18	1.66	0.43	1.72	0.19	1.65	0.43	1.72	0.19	1.66	0.42
747	1.72	0.19	1.66	0.43	1.72	0.19	1.66	0.43	1.72	0.19	1.66	0.42
748	1.72	0.19	1.67	0.43	1.72	0.19	1.66	0.43	1.72	0.19	1.66	0.42
749	1.72	0.19	1.67	0.43	1.72	0.19	1.66	0.43	1.72	0.19	1.66	0.42
750	1.72	0.19	1.67	0.43	1.72	0.19	1.66	0.43	1.72	0.19	1.66	0.42
751	1.72	0.19	1.67	0.43	1.72	0.19	1.66	0.43	1.72	0.19	1.66	0.42
752	1.72	0.19	1.67	0.43	1.72	0.19	1.66	0.42	1.72	0.19	1.66	0.42
753	1.72	0.19	1.67	0.43	1.72	0.19	1.66	0.42	1.72	0.19	1.66	0.42

754	1.72	0.19	1.67	0.43	1.72	0.19	1.66	0.42	1.72	0.19	1.66	0.42
755	1.72	0.19	1.67	0.43	1.72	0.19	1.66	0.42	1.72	0.20	1.66	0.42
756	1.72	0.19	1.67	0.43	1.72	0.19	1.66	0.42	1.72	0.20	1.66	0.42
757	1.72	0.19	1.67	0.43	1.72	0.19	1.66	0.42	1.72	0.20	1.66	0.42
758	1.72	0.19	1.67	0.43	1.72	0.19	1.66	0.42	1.72	0.20	1.66	0.42
759	1.72	0.19	1.67	0.43	1.72	0.19	1.66	0.42	1.72	0.20	1.66	0.42
760	1.72	0.19	1.67	0.42	1.72	0.19	1.66	0.42	1.72	0.20	1.66	0.42
761	1.72	0.19	1.67	0.42	1.72	0.19	1.66	0.42	1.72	0.20	1.66	0.42
762	1.72	0.19	1.67	0.42	1.72	0.20	1.66	0.42	1.72	0.20	1.66	0.42
763	1.72	0.19	1.67	0.42	1.72	0.20	1.66	0.42	1.72	0.20	1.66	0.42
764	1.72	0.19	1.67	0.42	1.72	0.20	1.66	0.42	1.72	0.20	1.66	0.42
765	1.72	0.19	1.67	0.42	1.72	0.20	1.66	0.42	1.72	0.20	1.66	0.42
766	1.72	0.19	1.67	0.42	1.72	0.20	1.66	0.42	1.72	0.20	1.66	0.42
767	1.73	0.19	1.67	0.42	1.72	0.20	1.66	0.42	1.72	0.20	1.66	0.42
768	1.73	0.19	1.67	0.42	1.72	0.20	1.66	0.42	1.72	0.20	1.66	0.42
769	1.73	0.19	1.67	0.42	1.72	0.20	1.66	0.42	1.72	0.20	1.66	0.42
770	1.73	0.20	1.67	0.42	1.72	0.20	1.66	0.42	1.72	0.20	1.66	0.42
771	1.73	0.20	1.67	0.42	1.72	0.20	1.66	0.42	1.72	0.20	1.66	0.42
772	1.73	0.20	1.67	0.42	1.72	0.20	1.66	0.43	1.72	0.20	1.66	0.42
773	1.73	0.20	1.67	0.42	1.72	0.20	1.66	0.43	1.72	0.20	1.66	0.42
774	1.73	0.20	1.67	0.42	1.72	0.20	1.66	0.43	1.72	0.20	1.65	0.43
775	1.73	0.20	1.67	0.43	1.72	0.20	1.66	0.43	1.72	0.20	1.65	0.43
776	1.73	0.20	1.66	0.43	1.72	0.20	1.65	0.43	1.72	0.20	1.65	0.43
777	1.73	0.20	1.66	0.43	1.72	0.20	1.65	0.43	1.72	0.20	1.65	0.43
778	1.73	0.20	1.66	0.43	1.73	0.20	1.65	0.43	1.72	0.20	1.65	0.43
779	1.73	0.20	1.66	0.43	1.73	0.20	1.65	0.43	1.72	0.20	1.65	0.43
780	1.73	0.20	1.66	0.43	1.73	0.20	1.65	0.43	1.72	0.20	1.65	0.43
781	1.73	0.20	1.66	0.43	1.73	0.20	1.65	0.43	1.72	0.21	1.65	0.43
782	1.73	0.20	1.66	0.43	1.73	0.20	1.65	0.43	1.72	0.21	1.65	0.43
783	1.73	0.20	1.66	0.43	1.73	0.20	1.65	0.43	1.72	0.21	1.65	0.43
784	1.73	0.20	1.66	0.43	1.73	0.20	1.65	0.43	1.72	0.21	1.64	0.43
785	1.73	0.20	1.65	0.43	1.73	0.20	1.65	0.44	1.72	0.21	1.64	0.44
786	1.73	0.20	1.65	0.44	1.73	0.20	1.65	0.44	1.73	0.21	1.64	0.44
787	1.73	0.20	1.65	0.44	1.73	0.20	1.64	0.44	1.73	0.21	1.64	0.44
788	1.73	0.20	1.65	0.44	1.73	0.20	1.64	0.44	1.73	0.21	1.64	0.44
789	1.73	0.20	1.65	0.44	1.73	0.21	1.64	0.44	1.73	0.21	1.64	0.44
790	1.73	0.20	1.65	0.44	1.73	0.21	1.64	0.44	1.73	0.21	1.64	0.44
791	1.73	0.20	1.65	0.44	1.73	0.21	1.64	0.44	1.73	0.21	1.64	0.44
792	1.73	0.20	1.65	0.44	1.73	0.21	1.64	0.45	1.73	0.21	1.64	0.45
793	1.73	0.20	1.65	0.45	1.73	0.21	1.64	0.45	1.73	0.21	1.64	0.45
794	1.73	0.20	1.65	0.45	1.73	0.21	1.64	0.45	1.73	0.21	1.63	0.45
795	1.73	0.20	1.65	0.45	1.73	0.21	1.64	0.45	1.73	0.21	1.63	0.45
796	1.73	0.20	1.64	0.45	1.73	0.21	1.64	0.45	1.73	0.21	1.63	0.45

797	1.73	0.20	1.64	0.45	1.73	0.21	1.64	0.45	1.73	0.21	1.63	0.45
798	1.73	0.20	1.64	0.46	1.73	0.21	1.63	0.46	1.73	0.21	1.63	0.46
799	1.73	0.20	1.64	0.46	1.73	0.21	1.63	0.46	1.73	0.21	1.63	0.46
800	1.73	0.20	1.64	0.46	1.73	0.21	1.63	0.46	1.73	0.21	1.63	0.46
801	1.73	0.20	1.64	0.46	1.73	0.21	1.63	0.46	1.73	0.21	1.63	0.46
802	1.73	0.20	1.64	0.46	1.73	0.21	1.63	0.46	1.73	0.21	1.63	0.46
803	1.73	0.20	1.64	0.47	1.73	0.21	1.63	0.46	1.73	0.21	1.63	0.46
804	1.73	0.20	1.64	0.47	1.73	0.21	1.63	0.47	1.73	0.21	1.63	0.47
805	1.73	0.20	1.64	0.47	1.73	0.21	1.63	0.47	1.73	0.21	1.63	0.47
806	1.73	0.20	1.64	0.47	1.73	0.21	1.63	0.47	1.73	0.21	1.63	0.47
807	1.73	0.21	1.64	0.47	1.73	0.21	1.63	0.47	1.73	0.21	1.62	0.47
808	1.73	0.21	1.64	0.48	1.73	0.21	1.63	0.48	1.73	0.21	1.62	0.47
809	1.73	0.21	1.64	0.48	1.73	0.21	1.63	0.48	1.73	0.22	1.62	0.48
810	1.73	0.21	1.64	0.48	1.73	0.21	1.63	0.48	1.73	0.22	1.62	0.48
811	1.73	0.21	1.64	0.48	1.73	0.21	1.63	0.48	1.73	0.22	1.62	0.48
812	1.73	0.21	1.64	0.49	1.73	0.21	1.63	0.48	1.73	0.22	1.62	0.48
813	1.73	0.21	1.64	0.49	1.73	0.21	1.63	0.49	1.73	0.22	1.62	0.49
814	1.73	0.21	1.64	0.49	1.73	0.21	1.63	0.49	1.73	0.22	1.62	0.49
815	1.73	0.21	1.64	0.49	1.73	0.21	1.63	0.49	1.73	0.22	1.62	0.49
816	1.73	0.21	1.64	0.49	1.73	0.22	1.63	0.49	1.73	0.22	1.62	0.49
817	1.73	0.21	1.64	0.50	1.73	0.22	1.62	0.49	1.73	0.22	1.62	0.49
818	1.73	0.21	1.64	0.50	1.73	0.22	1.62	0.50	1.73	0.22	1.62	0.50
819	1.73	0.21	1.64	0.50	1.73	0.22	1.62	0.50	1.73	0.22	1.62	0.50
820	1.73	0.21	1.64	0.50	1.73	0.22	1.62	0.50	1.73	0.22	1.62	0.50
821	1.73	0.21	1.64	0.51	1.73	0.22	1.62	0.50	1.73	0.22	1.62	0.50
822	1.73	0.21	1.64	0.51	1.73	0.22	1.62	0.51	1.73	0.22	1.62	0.51
823	1.73	0.21	1.64	0.51	1.73	0.22	1.62	0.51	1.73	0.22	1.62	0.51
824	1.73	0.21	1.64	0.51	1.73	0.22	1.62	0.51	1.73	0.22	1.62	0.51
825	1.73	0.21	1.64	0.52	1.73	0.22	1.62	0.51	1.73	0.22	1.62	0.51
826	1.73	0.21	1.64	0.52	1.73	0.22	1.62	0.51	1.73	0.22	1.62	0.51
827	1.73	0.21	1.64	0.52	1.73	0.22	1.62	0.52	1.73	0.22	1.62	0.52
828	1.73	0.21	1.64	0.52	1.73	0.22	1.62	0.52	1.73	0.22	1.62	0.52
829	1.73	0.21	1.64	0.52	1.73	0.22	1.62	0.52	1.73	0.22	1.62	0.52
830	1.73	0.21	1.64	0.53	1.73	0.22	1.62	0.52	1.73	0.22	1.62	0.52
831	1.73	0.21	1.64	0.53	1.73	0.22	1.62	0.53	1.73	0.22	1.62	0.53
832	1.73	0.21	1.64	0.53	1.73	0.22	1.63	0.53	1.73	0.22	1.62	0.53
833	1.73	0.22	1.64	0.53	1.73	0.22	1.63	0.53	1.73	0.22	1.62	0.53
834	1.73	0.22	1.64	0.54	1.73	0.22	1.63	0.53	1.73	0.22	1.62	0.53
835	1.73	0.22	1.64	0.54	1.73	0.22	1.63	0.54	1.73	0.23	1.62	0.53
836	1.73	0.22	1.64	0.54	1.73	0.22	1.63	0.54	1.73	0.23	1.62	0.54
837	1.73	0.22	1.64	0.54	1.73	0.22	1.63	0.54	1.73	0.23	1.62	0.54
838	1.73	0.22	1.64	0.54	1.73	0.22	1.63	0.54	1.73	0.23	1.62	0.54
839	1.73	0.22	1.64	0.55	1.73	0.22	1.63	0.54	1.73	0.23	1.62	0.54

840	1.73	0.22	1.64	0.55	1.73	0.22	1.63	0.55	1.73	0.23	1.62	0.55
841	1.73	0.22	1.64	0.55	1.73	0.23	1.63	0.55	1.73	0.23	1.62	0.55
842	1.73	0.22	1.64	0.55	1.73	0.23	1.63	0.55	1.73	0.23	1.62	0.55
843	1.73	0.22	1.64	0.55	1.73	0.23	1.63	0.55	1.73	0.23	1.62	0.55
844	1.73	0.22	1.65	0.56	1.73	0.23	1.63	0.56	1.73	0.23	1.62	0.56
845	1.73	0.22	1.65	0.56	1.73	0.23	1.63	0.56	1.73	0.23	1.62	0.56
846	1.73	0.22	1.65	0.56	1.73	0.23	1.63	0.56	1.73	0.23	1.62	0.56
847	1.73	0.22	1.65	0.56	1.73	0.23	1.63	0.56	1.73	0.23	1.62	0.56
848	1.73	0.22	1.65	0.57	1.73	0.23	1.63	0.56	1.73	0.23	1.62	0.56
849	1.73	0.22	1.65	0.57	1.73	0.23	1.63	0.57	1.73	0.23	1.62	0.57
850	1.73	0.22	1.65	0.57	1.73	0.23	1.63	0.57	1.73	0.23	1.63	0.57
851	1.73	0.22	1.65	0.57	1.73	0.23	1.63	0.57	1.73	0.23	1.63	0.57
852	1.73	0.22	1.65	0.57	1.73	0.23	1.63	0.57	1.73	0.23	1.63	0.57
853	1.73	0.22	1.65	0.58	1.73	0.23	1.63	0.58	1.73	0.23	1.63	0.58
854	1.73	0.23	1.65	0.58	1.73	0.23	1.63	0.58	1.73	0.23	1.63	0.58
855	1.73	0.23	1.65	0.58	1.73	0.23	1.63	0.58	1.73	0.23	1.63	0.58
856	1.73	0.23	1.65	0.58	1.73	0.23	1.64	0.58	1.73	0.23	1.63	0.58
857	1.73	0.23	1.65	0.58	1.73	0.23	1.64	0.58	1.73	0.23	1.63	0.58
858	1.73	0.23	1.66	0.59	1.73	0.23	1.64	0.59	1.73	0.23	1.63	0.59
859	1.73	0.23	1.66	0.59	1.73	0.23	1.64	0.59	1.73	0.24	1.63	0.59
860	1.73	0.23	1.66	0.59	1.73	0.23	1.64	0.59	1.73	0.24	1.63	0.59
861	1.73	0.23	1.66	0.59	1.73	0.23	1.64	0.59	1.73	0.24	1.63	0.59
862	1.73	0.23	1.66	0.59	1.73	0.23	1.64	0.60	1.73	0.24	1.63	0.60
863	1.73	0.23	1.66	0.59	1.73	0.23	1.64	0.60	1.73	0.24	1.63	0.60
864	1.73	0.23	1.66	0.60	1.73	0.24	1.64	0.60	1.73	0.24	1.63	0.60
865	1.73	0.23	1.66	0.60	1.73	0.24	1.64	0.60	1.73	0.24	1.63	0.60
866	1.73	0.23	1.66	0.60	1.73	0.24	1.64	0.60	1.73	0.24	1.63	0.60
867	1.73	0.23	1.66	0.60	1.73	0.24	1.64	0.61	1.73	0.24	1.63	0.61
868	1.73	0.23	1.66	0.60	1.73	0.24	1.64	0.61	1.73	0.24	1.64	0.61
869	1.73	0.23	1.66	0.61	1.73	0.24	1.64	0.61	1.73	0.24	1.64	0.61
870	1.73	0.23	1.66	0.61	1.73	0.24	1.65	0.61	1.73	0.24	1.64	0.61
871	1.73	0.23	1.67	0.61	1.73	0.24	1.65	0.61	1.73	0.24	1.64	0.62
872	1.73	0.23	1.67	0.61	1.73	0.24	1.65	0.62	1.73	0.24	1.64	0.62
873	1.73	0.24	1.67	0.61	1.73	0.24	1.65	0.62	1.73	0.24	1.64	0.62
874	1.73	0.24	1.67	0.62	1.73	0.24	1.65	0.62	1.73	0.24	1.64	0.62
875	1.73	0.24	1.67	0.62	1.73	0.24	1.65	0.62	1.73	0.24	1.64	0.62
876	1.73	0.24	1.67	0.62	1.73	0.24	1.65	0.63	1.73	0.24	1.64	0.63
877	1.73	0.24	1.67	0.62	1.73	0.24	1.65	0.63	1.73	0.24	1.64	0.63
878	1.73	0.24	1.67	0.62	1.73	0.24	1.65	0.63	1.73	0.24	1.64	0.63
879	1.73	0.24	1.67	0.63	1.73	0.24	1.65	0.63	1.73	0.24	1.64	0.63
880	1.73	0.24	1.67	0.63	1.73	0.24	1.65	0.63	1.73	0.24	1.64	0.64
881	1.73	0.24	1.67	0.63	1.73	0.24	1.65	0.64	1.73	0.25	1.65	0.64
882	1.73	0.24	1.67	0.63	1.73	0.24	1.66	0.64	1.73	0.25	1.65	0.64

883	1.73	0.24	1.68	0.63	1.73	0.24	1.66	0.64	1.73	0.25	1.65	0.64
884	1.73	0.24	1.68	0.64	1.73	0.25	1.66	0.64	1.73	0.25	1.65	0.65
885	1.73	0.24	1.68	0.64	1.73	0.25	1.66	0.65	1.73	0.25	1.65	0.65
886	1.73	0.24	1.68	0.64	1.73	0.25	1.66	0.65	1.73	0.25	1.65	0.65
887	1.73	0.24	1.68	0.64	1.73	0.25	1.66	0.65	1.73	0.25	1.65	0.65
888	1.73	0.24	1.68	0.65	1.73	0.25	1.66	0.65	1.73	0.25	1.65	0.65
889	1.73	0.24	1.68	0.65	1.73	0.25	1.66	0.65	1.73	0.25	1.65	0.66
890	1.73	0.24	1.68	0.65	1.73	0.25	1.66	0.66	1.73	0.25	1.65	0.66
891	1.73	0.25	1.68	0.65	1.73	0.25	1.66	0.66	1.73	0.25	1.65	0.66
892	1.73	0.25	1.68	0.65	1.73	0.25	1.67	0.66	1.73	0.25	1.66	0.66
893	1.73	0.25	1.69	0.66	1.73	0.25	1.67	0.66	1.73	0.25	1.66	0.67
894	1.73	0.25	1.69	0.66	1.73	0.25	1.67	0.67	1.73	0.25	1.66	0.67
895	1.73	0.25	1.69	0.66	1.73	0.25	1.67	0.67	1.73	0.25	1.66	0.67
896	1.73	0.25	1.69	0.66	1.73	0.25	1.67	0.67	1.73	0.25	1.66	0.67
897	1.73	0.25	1.69	0.66	1.73	0.25	1.67	0.67	1.73	0.25	1.66	0.68
898	1.73	0.25	1.69	0.67	1.73	0.25	1.67	0.68	1.73	0.25	1.66	0.68
899	1.73	0.25	1.69	0.67	1.73	0.25	1.67	0.68	1.73	0.25	1.66	0.68
900	1.73	0.25	1.69	0.67	1.73	0.25	1.67	0.68	1.73	0.26	1.66	0.68
901	1.73	0.25	1.69	0.67	1.73	0.25	1.68	0.68	1.73	0.26	1.67	0.69
902	1.73	0.25	1.70	0.68	1.73	0.26	1.68	0.68	1.73	0.26	1.67	0.69
903	1.73	0.25	1.70	0.68	1.73	0.26	1.68	0.69	1.73	0.26	1.67	0.69
904	1.73	0.25	1.70	0.68	1.73	0.26	1.68	0.69	1.73	0.26	1.67	0.69
905	1.74	0.25	1.70	0.68	1.73	0.26	1.68	0.69	1.73	0.26	1.67	0.70
906	1.74	0.25	1.70	0.69	1.73	0.26	1.68	0.69	1.73	0.26	1.67	0.70
907	1.74	0.26	1.70	0.69	1.73	0.26	1.68	0.70	1.73	0.26	1.67	0.70
908	1.74	0.26	1.70	0.69	1.73	0.26	1.69	0.70	1.73	0.26	1.68	0.70
909	1.74	0.26	1.71	0.69	1.73	0.26	1.69	0.70	1.73	0.26	1.68	0.70
910	1.74	0.26	1.71	0.69	1.73	0.26	1.69	0.70	1.73	0.26	1.68	0.71
911	1.74	0.26	1.71	0.70	1.73	0.26	1.69	0.71	1.73	0.26	1.68	0.71
912	1.74	0.26	1.71	0.70	1.73	0.26	1.69	0.71	1.73	0.26	1.68	0.71
913	1.74	0.26	1.71	0.70	1.73	0.26	1.69	0.71	1.73	0.26	1.68	0.71
914	1.74	0.26	1.71	0.70	1.73	0.26	1.69	0.71	1.73	0.26	1.68	0.72
915	1.74	0.26	1.71	0.71	1.73	0.26	1.70	0.72	1.73	0.26	1.69	0.72
916	1.74	0.26	1.72	0.71	1.73	0.26	1.70	0.72	1.73	0.27	1.69	0.72
917	1.74	0.26	1.72	0.71	1.73	0.26	1.70	0.72	1.73	0.27	1.69	0.72
918	1.74	0.26	1.72	0.71	1.73	0.27	1.70	0.72	1.73	0.27	1.69	0.73
919	1.74	0.26	1.72	0.71	1.74	0.27	1.70	0.72	1.73	0.27	1.69	0.73
920	1.74	0.26	1.72	0.72	1.74	0.27	1.70	0.73	1.73	0.27	1.69	0.73
921	1.74	0.27	1.73	0.72	1.74	0.27	1.71	0.73	1.73	0.27	1.70	0.73
922	1.74	0.27	1.73	0.72	1.74	0.27	1.71	0.73	1.73	0.27	1.70	0.74
923	1.74	0.27	1.73	0.72	1.74	0.27	1.71	0.73	1.73	0.27	1.70	0.74
924	1.74	0.27	1.73	0.73	1.74	0.27	1.71	0.74	1.73	0.27	1.70	0.74
925	1.74	0.27	1.73	0.73	1.74	0.27	1.71	0.74	1.73	0.27	1.70	0.74

926	1.74	0.27	1.73	0.73	1.74	0.27	1.72	0.74	1.73	0.27	1.71	0.75
927	1.74	0.27	1.74	0.73	1.74	0.27	1.72	0.74	1.73	0.27	1.71	0.75
928	1.74	0.27	1.74	0.73	1.74	0.27	1.72	0.75	1.73	0.27	1.71	0.75
929	1.74	0.27	1.74	0.74	1.74	0.27	1.72	0.75	1.73	0.27	1.71	0.75
930	1.74	0.27	1.74	0.74	1.74	0.27	1.72	0.75	1.74	0.27	1.71	0.75
931	1.74	0.27	1.75	0.74	1.74	0.27	1.73	0.75	1.74	0.28	1.72	0.76
932	1.74	0.27	1.75	0.74	1.74	0.28	1.73	0.75	1.74	0.28	1.72	0.76
933	1.74	0.27	1.75	0.75	1.74	0.28	1.73	0.76	1.74	0.28	1.72	0.76
934	1.74	0.27	1.75	0.75	1.74	0.28	1.73	0.76	1.74	0.28	1.72	0.76
935	1.74	0.28	1.75	0.75	1.74	0.28	1.74	0.76	1.74	0.28	1.72	0.77
936	1.74	0.28	1.76	0.75	1.74	0.28	1.74	0.76	1.74	0.28	1.73	0.77
937	1.74	0.28	1.76	0.75	1.74	0.28	1.74	0.76	1.74	0.28	1.73	0.77
938	1.74	0.28	1.76	0.76	1.74	0.28	1.74	0.77	1.74	0.28	1.73	0.77
939	1.74	0.28	1.76	0.76	1.74	0.28	1.75	0.77	1.74	0.28	1.73	0.77
940	1.74	0.28	1.77	0.76	1.74	0.28	1.75	0.77	1.74	0.28	1.74	0.78
941	1.74	0.28	1.77	0.76	1.74	0.28	1.75	0.77	1.74	0.28	1.74	0.78
942	1.74	0.28	1.77	0.76	1.74	0.28	1.75	0.78	1.74	0.28	1.74	0.78
943	1.74	0.28	1.77	0.77	1.74	0.28	1.75	0.78	1.74	0.29	1.74	0.78
944	1.74	0.28	1.78	0.77	1.74	0.29	1.76	0.78	1.74	0.29	1.75	0.78
945	1.74	0.28	1.78	0.77	1.74	0.29	1.76	0.78	1.74	0.29	1.75	0.79
946	1.74	0.29	1.78	0.77	1.74	0.29	1.76	0.78	1.74	0.29	1.75	0.79
947	1.74	0.29	1.78	0.77	1.74	0.29	1.77	0.78	1.74	0.29	1.75	0.79
948	1.74	0.29	1.79	0.77	1.74	0.29	1.77	0.79	1.74	0.29	1.76	0.79
949	1.74	0.29	1.79	0.78	1.74	0.29	1.77	0.79	1.74	0.29	1.76	0.79
950	1.75	0.29	1.79	0.78	1.74	0.29	1.77	0.79	1.74	0.29	1.76	0.80
951	1.75	0.29	1.79	0.78	1.74	0.29	1.78	0.79	1.74	0.29	1.76	0.80
952	1.75	0.29	1.80	0.78	1.74	0.29	1.78	0.79	1.74	0.29	1.77	0.80
953	1.75	0.29	1.80	0.78	1.74	0.29	1.78	0.80	1.74	0.29	1.77	0.80
954	1.75	0.29	1.80	0.78	1.74	0.29	1.78	0.80	1.74	0.30	1.77	0.80
955	1.75	0.29	1.81	0.79	1.74	0.30	1.79	0.80	1.74	0.30	1.77	0.81
956	1.75	0.29	1.81	0.79	1.74	0.30	1.79	0.80	1.74	0.30	1.78	0.81
957	1.75	0.29	1.81	0.79	1.74	0.30	1.79	0.80	1.74	0.30	1.78	0.81
958	1.75	0.30	1.81	0.79	1.74	0.30	1.80	0.80	1.74	0.30	1.78	0.81
959	1.75	0.30	1.82	0.79	1.74	0.30	1.80	0.80	1.74	0.30	1.79	0.81
960	1.75	0.30	1.82	0.79	1.74	0.30	1.80	0.81	1.74	0.30	1.79	0.81
961	1.75	0.30	1.82	0.79	1.75	0.30	1.80	0.81	1.74	0.30	1.79	0.82
962	1.75	0.30	1.83	0.80	1.75	0.30	1.81	0.81	1.74	0.30	1.79	0.82
963	1.75	0.30	1.83	0.80	1.75	0.30	1.81	0.81	1.74	0.30	1.80	0.82
964	1.75	0.30	1.83	0.80	1.75	0.30	1.81	0.81	1.74	0.30	1.80	0.82
965	1.75	0.30	1.84	0.80	1.75	0.30	1.82	0.81	1.74	0.31	1.80	0.82
966	1.75	0.30	1.84	0.80	1.75	0.31	1.82	0.81	1.75	0.31	1.81	0.82
967	1.75	0.30	1.84	0.80	1.75	0.31	1.82	0.82	1.75	0.31	1.81	0.82
968	1.75	0.31	1.84	0.80	1.75	0.31	1.83	0.82	1.75	0.31	1.81	0.83

969	1.75	0.31	1.85	0.80	1.75	0.31	1.83	0.82	1.75	0.31	1.82	0.83
970	1.76	0.31	1.85	0.80	1.75	0.31	1.83	0.82	1.75	0.31	1.82	0.83
971	1.76	0.31	1.85	0.80	1.75	0.31	1.83	0.82	1.75	0.31	1.82	0.83
972	1.76	0.31	1.86	0.81	1.75	0.31	1.84	0.82	1.75	0.31	1.82	0.83
973	1.76	0.31	1.86	0.81	1.75	0.31	1.84	0.82	1.75	0.31	1.83	0.83
974	1.76	0.31	1.86	0.81	1.75	0.31	1.84	0.82	1.75	0.31	1.83	0.83
975	1.76	0.31	1.87	0.81	1.75	0.32	1.85	0.82	1.75	0.32	1.83	0.83
976	1.76	0.31	1.87	0.81	1.75	0.32	1.85	0.82	1.75	0.32	1.84	0.83
977	1.76	0.31	1.87	0.81	1.75	0.32	1.85	0.83	1.75	0.32	1.84	0.84
978	1.76	0.32	1.87	0.81	1.75	0.32	1.86	0.83	1.75	0.32	1.84	0.84
979	1.76	0.32	1.88	0.81	1.76	0.32	1.86	0.83	1.75	0.32	1.85	0.84
980	1.76	0.32	1.88	0.81	1.76	0.32	1.86	0.83	1.75	0.32	1.85	0.84
981	1.76	0.32	1.88	0.81	1.76	0.32	1.86	0.83	1.75	0.32	1.85	0.84
982	1.76	0.32	1.89	0.81	1.76	0.32	1.87	0.83	1.75	0.32	1.86	0.84
983	1.77	0.32	1.89	0.81	1.76	0.32	1.87	0.83	1.76	0.32	1.86	0.84
984	1.77	0.32	1.89	0.81	1.76	0.32	1.87	0.83	1.76	0.33	1.86	0.84
985	1.77	0.32	1.90	0.81	1.76	0.33	1.88	0.83	1.76	0.33	1.86	0.84
986	1.77	0.32	1.90	0.81	1.76	0.33	1.88	0.83	1.76	0.33	1.87	0.84
987	1.77	0.32	1.90	0.82	1.76	0.33	1.88	0.83	1.76	0.33	1.87	0.84
988	1.77	0.33	1.91	0.82	1.76	0.33	1.89	0.83	1.76	0.33	1.87	0.84
989	1.77	0.33	1.91	0.82	1.76	0.33	1.89	0.83	1.76	0.33	1.88	0.84
990	1.77	0.33	1.91	0.82	1.76	0.33	1.89	0.83	1.76	0.33	1.88	0.85
991	1.77	0.33	1.91	0.82	1.77	0.33	1.90	0.83	1.76	0.33	1.88	0.85
992	1.77	0.33	1.92	0.82	1.77	0.33	1.90	0.83	1.76	0.33	1.89	0.85
993	1.77	0.33	1.92	0.82	1.77	0.33	1.90	0.84	1.76	0.34	1.89	0.85
994	1.78	0.33	1.92	0.82	1.77	0.34	1.91	0.84	1.77	0.34	1.89	0.85
995	1.78	0.33	1.93	0.82	1.77	0.34	1.91	0.84	1.77	0.34	1.90	0.85
996	1.78	0.33	1.93	0.82	1.77	0.34	1.91	0.84	1.77	0.34	1.90	0.85
997	1.78	0.33	1.93	0.82	1.77	0.34	1.91	0.84	1.77	0.34	1.90	0.85
998	1.78	0.33	1.94	0.82	1.77	0.34	1.92	0.84	1.77	0.34	1.91	0.85
999	1.78	0.34	1.94	0.82	1.77	0.34	1.92	0.84	1.77	0.34	1.91	0.85
1000	1.78	0.34	1.94	0.82	1.78	0.34	1.92	0.84	1.77	0.34	1.91	0.85
1006	1.79	0.34	1.96	0.82	1.78	0.35	1.94	0.84	1.78	0.35	1.93	0.85
1012	1.80	0.35	1.98	0.82	1.79	0.35	1.96	0.84	1.79	0.35	1.95	0.85
1018	1.81	0.35	1.99	0.81	1.80	0.36	1.98	0.83	1.80	0.36	1.97	0.85
1024	1.82	0.35	2.01	0.81	1.81	0.36	2.00	0.83	1.81	0.36	1.99	0.85
1030	1.83	0.35	2.03	0.81	1.82	0.36	2.01	0.83	1.82	0.37	2.00	0.84
1036	1.84	0.36	2.04	0.80	1.83	0.36	2.03	0.82	1.83	0.37	2.02	0.84
1042	1.85	0.36	2.06	0.79	1.84	0.37	2.05	0.82	1.84	0.37	2.04	0.84
1048	1.86	0.35	2.07	0.79	1.85	0.36	2.06	0.81	1.85	0.37	2.05	0.83
1054	1.87	0.35	2.09	0.78	1.86	0.36	2.08	0.81	1.86	0.37	2.07	0.82
1060	1.88	0.35	2.10	0.77	1.87	0.36	2.09	0.80	1.87	0.36	2.09	0.81
1066	1.88	0.35	2.12	0.76	1.88	0.36	2.11	0.79	1.88	0.36	2.10	0.81

1072	1.89	0.34	2.13	0.75	1.89	0.35	2.12	0.78	1.89	0.36	2.12	0.80
1078	1.90	0.34	2.14	0.74	1.90	0.35	2.13	0.77	1.90	0.35	2.13	0.79
1084	1.91	0.33	2.15	0.73	1.91	0.34	2.14	0.76	1.91	0.34	2.14	0.77
1090	1.91	0.33	2.16	0.72	1.91	0.33	2.16	0.75	1.91	0.34	2.15	0.76
1096	1.92	0.32	2.17	0.71	1.92	0.33	2.17	0.74	1.92	0.33	2.16	0.75
1102	1.92	0.31	2.18	0.70	1.92	0.32	2.17	0.72	1.92	0.32	2.17	0.74
1108	1.93	0.31	2.19	0.69	1.93	0.31	2.18	0.71	1.93	0.32	2.18	0.72
1114	1.93	0.30	2.19	0.67	1.93	0.31	2.19	0.70	1.93	0.31	2.18	0.71
1120	1.93	0.30	2.20	0.66	1.93	0.30	2.19	0.69	1.93	0.30	2.19	0.70
1126	1.93	0.29	2.20	0.65	1.94	0.30	2.20	0.67	1.94	0.30	2.19	0.68
1132	1.94	0.29	2.21	0.64	1.94	0.29	2.20	0.66	1.94	0.29	2.20	0.67
1138	1.94	0.28	2.21	0.62	1.94	0.28	2.20	0.65	1.94	0.29	2.20	0.66
1144	1.94	0.28	2.21	0.61	1.94	0.28	2.20	0.64	1.94	0.28	2.20	0.65
1150	1.94	0.27	2.21	0.60	1.94	0.27	2.20	0.62	1.94	0.28	2.20	0.64
1156	1.94	0.27	2.21	0.59	1.94	0.27	2.20	0.61	1.94	0.27	2.20	0.62
1162	1.94	0.26	2.21	0.58	1.94	0.27	2.20	0.60	1.94	0.27	2.20	0.61
1168	1.94	0.26	2.21	0.57	1.94	0.26	2.20	0.59	1.94	0.26	2.19	0.60
1174	1.94	0.26	2.21	0.56	1.94	0.26	2.20	0.58	1.94	0.26	2.19	0.60
1180	1.94	0.25	2.20	0.55	1.94	0.25	2.20	0.57	1.94	0.26	2.19	0.59
1186	1.94	0.25	2.20	0.55	1.94	0.25	2.19	0.57	1.94	0.25	2.18	0.58
1192	1.94	0.24	2.20	0.54	1.94	0.25	2.19	0.56	1.94	0.25	2.18	0.57
1198	1.94	0.24	2.19	0.53	1.94	0.24	2.19	0.55	1.94	0.25	2.18	0.57
1204	1.94	0.24	2.19	0.52	1.94	0.24	2.18	0.55	1.94	0.24	2.17	0.56
1210	1.94	0.24	2.19	0.52	1.94	0.24	2.18	0.54	1.94	0.24	2.17	0.55
1216	1.94	0.23	2.18	0.51	1.94	0.24	2.17	0.54	1.94	0.24	2.16	0.55
1222	1.94	0.23	2.18	0.51	1.94	0.23	2.17	0.53	1.94	0.23	2.16	0.55
1228	1.94	0.23	2.17	0.50	1.94	0.23	2.16	0.53	1.94	0.23	2.15	0.54
1234	1.94	0.23	2.17	0.50	1.94	0.23	2.16	0.52	1.94	0.23	2.15	0.54
1240	1.94	0.22	2.16	0.50	1.94	0.23	2.15	0.52	1.93	0.23	2.14	0.54
1246	1.94	0.22	2.16	0.49	1.94	0.22	2.15	0.52	1.93	0.23	2.14	0.54
1252	1.94	0.22	2.16	0.49	1.93	0.22	2.14	0.52	1.93	0.22	2.13	0.53
1258	1.94	0.22	2.15	0.49	1.93	0.22	2.14	0.51	1.93	0.22	2.13	0.53
1264	1.93	0.22	2.15	0.49	1.93	0.22	2.14	0.51	1.93	0.22	2.12	0.53
1270	1.93	0.22	2.14	0.49	1.93	0.22	2.13	0.51	1.93	0.22	2.12	0.53
1276	1.93	0.21	2.14	0.48	1.93	0.22	2.13	0.51	1.93	0.22	2.11	0.53
1282	1.93	0.21	2.14	0.48	1.93	0.21	2.12	0.51	1.93	0.22	2.11	0.53
1288	1.93	0.21	2.13	0.48	1.93	0.21	2.12	0.51	1.93	0.22	2.10	0.53
1294	1.93	0.21	2.13	0.48	1.93	0.21	2.11	0.51	1.93	0.21	2.10	0.54
1300	1.93	0.21	2.12	0.48	1.93	0.21	2.11	0.51	1.93	0.21	2.10	0.54
1306	1.93	0.21	2.12	0.48	1.93	0.21	2.11	0.52	1.93	0.21	2.09	0.54
1312	1.93	0.21	2.12	0.48	1.93	0.21	2.10	0.52	1.92	0.21	2.09	0.54
1318	1.93	0.21	2.11	0.49	1.93	0.21	2.10	0.52	1.92	0.21	2.09	0.54
1324	1.93	0.20	2.11	0.49	1.92	0.21	2.10	0.52	1.92	0.21	2.08	0.55

1330	1.93	0.20	2.11	0.49	1.92	0.21	2.09	0.52	1.92	0.21	2.08	0.55
1336	1.93	0.20	2.11	0.49	1.92	0.21	2.09	0.53	1.92	0.21	2.08	0.55
1342	1.92	0.20	2.10	0.49	1.92	0.20	2.09	0.53	1.92	0.21	2.07	0.56
1348	1.92	0.20	2.10	0.49	1.92	0.20	2.09	0.53	1.92	0.21	2.07	0.56
1354	1.92	0.20	2.10	0.49	1.92	0.20	2.08	0.53	1.92	0.21	2.07	0.57
1360	1.92	0.20	2.10	0.50	1.92	0.20	2.08	0.54	1.92	0.21	2.07	0.57
1366	1.92	0.20	2.10	0.50	1.92	0.20	2.08	0.54	1.92	0.21	2.07	0.57
1372	1.92	0.20	2.09	0.50	1.92	0.20	2.08	0.55	1.92	0.21	2.07	0.58
1378	1.92	0.20	2.09	0.50	1.92	0.20	2.08	0.55	1.92	0.21	2.06	0.58
1384	1.92	0.20	2.09	0.51	1.92	0.20	2.08	0.55	1.92	0.21	2.06	0.59
1390	1.92	0.20	2.09	0.51	1.92	0.20	2.08	0.56	1.91	0.21	2.06	0.59
1396	1.92	0.20	2.09	0.51	1.91	0.20	2.08	0.56	1.91	0.21	2.06	0.60
1402	1.92	0.20	2.09	0.51	1.91	0.20	2.08	0.56	1.91	0.21	2.06	0.60
1408	1.92	0.20	2.09	0.52	1.91	0.20	2.08	0.57	1.91	0.21	2.06	0.61
1414	1.92	0.20	2.09	0.52	1.91	0.20	2.08	0.57	1.91	0.21	2.06	0.61
1420	1.92	0.20	2.09	0.52	1.91	0.20	2.08	0.58	1.91	0.21	2.07	0.62
1426	1.91	0.20	2.09	0.53	1.91	0.20	2.08	0.58	1.91	0.21	2.07	0.62
1432	1.91	0.20	2.09	0.53	1.91	0.20	2.08	0.59	1.91	0.21	2.07	0.63
1438	1.91	0.20	2.09	0.53	1.91	0.20	2.08	0.59	1.91	0.21	2.07	0.64
1444	1.91	0.20	2.09	0.53	1.91	0.20	2.08	0.59	1.91	0.21	2.07	0.64
1450	1.91	0.20	2.09	0.54	1.91	0.20	2.08	0.60	1.91	0.21	2.07	0.65
1456	1.91	0.20	2.09	0.54	1.91	0.20	2.09	0.60	1.91	0.21	2.08	0.65
1462	1.91	0.20	2.09	0.54	1.91	0.20	2.09	0.61	1.91	0.21	2.08	0.66
1468	1.91	0.20	2.10	0.55	1.91	0.20	2.09	0.61	1.91	0.21	2.08	0.66
1474	1.91	0.20	2.10	0.55	1.91	0.21	2.09	0.62	1.91	0.21	2.09	0.67
1480	1.91	0.20	2.10	0.55	1.91	0.21	2.10	0.62	1.91	0.21	2.09	0.67
1486	1.91	0.20	2.10	0.56	1.91	0.21	2.10	0.62	1.91	0.21	2.09	0.68
1492	1.91	0.20	2.10	0.56	1.91	0.21	2.10	0.63	1.91	0.21	2.10	0.68
1498	1.91	0.20	2.11	0.56	1.91	0.21	2.11	0.63	1.91	0.21	2.10	0.69
1504	1.91	0.20	2.11	0.56	1.91	0.21	2.11	0.64	1.91	0.21	2.11	0.69
1510	1.91	0.20	2.11	0.57	1.91	0.21	2.11	0.64	1.91	0.21	2.11	0.70
1516	1.91	0.20	2.11	0.57	1.91	0.21	2.12	0.64	1.91	0.21	2.12	0.70
1522	1.91	0.21	2.11	0.57	1.91	0.21	2.12	0.65	1.91	0.21	2.12	0.71
1528	1.91	0.21	2.12	0.57	1.91	0.21	2.12	0.65	1.91	0.21	2.13	0.71
1534	1.91	0.21	2.12	0.57	1.91	0.21	2.13	0.65	1.91	0.21	2.13	0.71
1540	1.91	0.21	2.12	0.58	1.91	0.21	2.13	0.66	1.91	0.22	2.14	0.72
1546	1.91	0.21	2.13	0.58	1.91	0.21	2.14	0.66	1.91	0.22	2.14	0.72
1552	1.91	0.21	2.13	0.58	1.91	0.22	2.14	0.66	1.91	0.22	2.15	0.72
1558	1.91	0.21	2.13	0.58	1.91	0.22	2.15	0.66	1.91	0.22	2.15	0.73
1564	1.91	0.21	2.14	0.58	1.91	0.22	2.15	0.67	1.91	0.22	2.16	0.73
1570	1.91	0.21	2.14	0.59	1.91	0.22	2.16	0.67	1.91	0.22	2.17	0.73
1576	1.91	0.21	2.14	0.59	1.91	0.22	2.16	0.67	1.91	0.22	2.17	0.74
1582	1.91	0.21	2.15	0.59	1.91	0.22	2.17	0.67	1.91	0.22	2.18	0.74

1588	1.91	0.22	2.15	0.59	1.91	0.22	2.17	0.68	1.91	0.22	2.19	0.74
1594	1.91	0.22	2.15	0.59	1.91	0.22	2.18	0.68	1.91	0.22	2.19	0.74
1600	1.91	0.22	2.16	0.59	1.91	0.22	2.19	0.68	1.91	0.22	2.20	0.75
1606	1.91	0.22	2.16	0.59	1.91	0.22	2.19	0.68	1.91	0.23	2.21	0.75
1612	1.91	0.22	2.16	0.59	1.91	0.23	2.20	0.68	1.91	0.23	2.21	0.75
1618	1.91	0.22	2.17	0.59	1.91	0.23	2.20	0.68	1.91	0.23	2.22	0.75
1624	1.91	0.22	2.17	0.59	1.91	0.23	2.21	0.68	1.91	0.23	2.23	0.75
1630	1.91	0.22	2.18	0.59	1.91	0.23	2.21	0.68	1.91	0.23	2.24	0.75
1636	1.91	0.22	2.18	0.59	1.91	0.23	2.22	0.68	1.91	0.23	2.24	0.75
1642	1.91	0.23	2.18	0.59	1.91	0.23	2.23	0.68	1.92	0.23	2.25	0.75
1648	1.91	0.23	2.19	0.59	1.91	0.23	2.23	0.68	1.92	0.23	2.26	0.75
1654	1.91	0.23	2.19	0.59	1.91	0.23	2.24	0.68	1.92	0.23	2.26	0.75
1660	1.91	0.23	2.20	0.59	1.92	0.23	2.24	0.68	1.92	0.23	2.27	0.75
1666	1.91	0.23	2.20	0.59	1.92	0.23	2.25	0.68	1.92	0.23	2.28	0.75
1672	1.91	0.23	2.20	0.59	1.92	0.24	2.25	0.68	1.92	0.23	2.29	0.75
1678	1.91	0.23	2.21	0.59	1.92	0.24	2.26	0.68	1.92	0.24	2.29	0.75
1684	1.91	0.23	2.21	0.59	1.92	0.24	2.27	0.68	1.92	0.24	2.30	0.75
1690	1.91	0.23	2.21	0.59	1.92	0.24	2.27	0.68	1.92	0.24	2.31	0.75
1696	1.92	0.24	2.22	0.59	1.92	0.24	2.28	0.68	1.92	0.24	2.31	0.75
1702	1.92	0.24	2.22	0.59	1.92	0.24	2.28	0.68	1.93	0.24	2.32	0.75
1708	1.92	0.24	2.22	0.59	1.92	0.24	2.29	0.68	1.93	0.24	2.33	0.74
1714	1.92	0.24	2.23	0.59	1.93	0.24	2.29	0.67	1.93	0.24	2.33	0.74
1720	1.92	0.24	2.23	0.58	1.93	0.24	2.30	0.67	1.93	0.24	2.34	0.74
1726	1.92	0.24	2.24	0.58	1.93	0.24	2.30	0.67	1.93	0.24	2.35	0.74
1732	1.92	0.24	2.24	0.58	1.93	0.25	2.31	0.67	1.93	0.24	2.35	0.74
1738	1.92	0.24	2.24	0.58	1.93	0.25	2.31	0.67	1.93	0.24	2.36	0.73
1744	1.92	0.24	2.25	0.58	1.93	0.25	2.32	0.66	1.93	0.24	2.36	0.73
1750	1.93	0.25	2.25	0.58	1.93	0.25	2.32	0.66	1.94	0.24	2.37	0.73
1756	1.93	0.25	2.25	0.57	1.94	0.25	2.33	0.66	1.94	0.24	2.38	0.72
1762	1.93	0.25	2.25	0.57	1.94	0.25	2.33	0.66	1.94	0.25	2.38	0.72
1768	1.93	0.25	2.26	0.57	1.94	0.25	2.34	0.65	1.94	0.25	2.39	0.72
1774	1.93	0.25	2.26	0.57	1.94	0.25	2.34	0.65	1.94	0.25	2.39	0.72
1780	1.93	0.25	2.26	0.57	1.94	0.25	2.35	0.65	1.94	0.25	2.40	0.71
1786	1.93	0.25	2.27	0.56	1.94	0.25	2.35	0.64	1.94	0.25	2.40	0.71
1792	1.94	0.25	2.27	0.56	1.94	0.25	2.35	0.64	1.95	0.25	2.41	0.71
1798	1.94	0.25	2.27	0.56	1.95	0.25	2.36	0.64	1.95	0.25	2.41	0.70
1804	1.94	0.25	2.27	0.56	1.95	0.25	2.36	0.63	1.95	0.25	2.42	0.70
1810	1.94	0.25	2.28	0.56	1.95	0.25	2.37	0.63	1.95	0.25	2.42	0.69
1816	1.94	0.26	2.28	0.55	1.95	0.25	2.37	0.63	1.95	0.25	2.43	0.69
1822	1.94	0.26	2.28	0.55	1.95	0.25	2.37	0.62	1.95	0.25	2.43	0.69
1828	1.95	0.26	2.28	0.55	1.96	0.25	2.38	0.62	1.96	0.25	2.44	0.68
1834	1.95	0.26	2.29	0.55	1.96	0.25	2.38	0.62	1.96	0.25	2.44	0.68
1840	1.95	0.26	2.29	0.54	1.96	0.25	2.38	0.61	1.96	0.25	2.45	0.67

1846	1.95	0.26	2.29	0.54	1.96	0.25	2.39	0.61	1.96	0.25	2.45	0.67
1852	1.95	0.26	2.29	0.54	1.96	0.25	2.39	0.61	1.96	0.25	2.45	0.67
1858	1.95	0.26	2.30	0.53	1.96	0.25	2.39	0.60	1.96	0.25	2.46	0.66
1864	1.96	0.26	2.30	0.53	1.97	0.25	2.40	0.60	1.97	0.25	2.46	0.66
1870	1.96	0.26	2.30	0.53	1.97	0.25	2.40	0.60	1.97	0.25	2.47	0.65
1876	1.96	0.26	2.30	0.53	1.97	0.25	2.40	0.59	1.97	0.25	2.47	0.65
1882	1.96	0.26	2.30	0.52	1.97	0.25	2.40	0.59	1.97	0.25	2.47	0.64
1888	1.96	0.26	2.30	0.52	1.97	0.25	2.41	0.59	1.97	0.25	2.48	0.64
1894	1.97	0.26	2.31	0.52	1.98	0.25	2.41	0.58	1.97	0.25	2.48	0.64
1900	1.97	0.26	2.31	0.52	1.98	0.25	2.41	0.58	1.98	0.25	2.48	0.63
1906	1.97	0.26	2.31	0.51	1.98	0.25	2.41	0.57	1.98	0.25	2.49	0.63
1912	1.97	0.26	2.31	0.51	1.98	0.25	2.42	0.57	1.98	0.25	2.49	0.62
1918	1.97	0.26	2.31	0.51	1.98	0.25	2.42	0.57	1.98	0.25	2.49	0.62
1924	1.98	0.26	2.31	0.50	1.98	0.25	2.42	0.56	1.98	0.25	2.49	0.61
1930	1.98	0.26	2.31	0.50	1.99	0.25	2.42	0.56	1.98	0.25	2.50	0.61
1936	1.98	0.26	2.31	0.50	1.99	0.25	2.42	0.55	1.99	0.25	2.50	0.60
1942	1.98	0.26	2.32	0.50	1.99	0.25	2.43	0.55	1.99	0.25	2.50	0.60
1948	1.98	0.26	2.32	0.49	1.99	0.25	2.43	0.55	1.99	0.24	2.50	0.60
1954	1.98	0.26	2.32	0.49	1.99	0.25	2.43	0.54	1.99	0.24	2.50	0.59
1960	1.99	0.26	2.32	0.49	1.99	0.25	2.43	0.54	1.99	0.24	2.51	0.59
1966	1.99	0.26	2.32	0.48	2.00	0.25	2.43	0.54	1.99	0.24	2.51	0.58
1972	1.99	0.26	2.32	0.48	2.00	0.25	2.43	0.53	1.99	0.24	2.51	0.58
1978	1.99	0.26	2.32	0.48	2.00	0.25	2.43	0.53	2.00	0.24	2.51	0.57
1984	1.99	0.26	2.32	0.48	2.00	0.25	2.44	0.52	2.00	0.24	2.51	0.57
1990	2.00	0.26	2.32	0.47	2.00	0.25	2.44	0.52	2.00	0.24	2.52	0.56
1996	2.00	0.26	2.32	0.47	2.00	0.25	2.44	0.52	2.00	0.24	2.52	0.56
2002	2.00	0.26	2.32	0.47	2.01	0.24	2.44	0.51	2.00	0.24	2.52	0.56
2008	2.00	0.26	2.32	0.46	2.01	0.24	2.44	0.51	2.00	0.24	2.52	0.55
2014	2.00	0.26	2.32	0.46	2.01	0.24	2.44	0.51	2.01	0.24	2.52	0.55
2020	2.01	0.26	2.32	0.46	2.01	0.24	2.44	0.50	2.01	0.24	2.52	0.54
2026	2.01	0.26	2.32	0.46	2.01	0.24	2.44	0.50	2.01	0.24	2.52	0.54
2032	2.01	0.25	2.32	0.45	2.01	0.24	2.44	0.50	2.01	0.24	2.52	0.54
2038	2.01	0.25	2.32	0.45	2.02	0.24	2.44	0.49	2.01	0.23	2.52	0.53
2044	2.01	0.25	2.32	0.45	2.02	0.24	2.44	0.49	2.01	0.23	2.53	0.53
2050	2.01	0.25	2.32	0.45	2.02	0.24	2.44	0.49	2.01	0.23	2.53	0.52
2056	2.02	0.25	2.32	0.44	2.02	0.24	2.45	0.48	2.01	0.23	2.53	0.52
2062	2.02	0.25	2.32	0.44	2.02	0.24	2.45	0.48	2.02	0.23	2.53	0.52
2068	2.02	0.25	2.32	0.44	2.02	0.24	2.45	0.47	2.02	0.23	2.53	0.51
2074	2.02	0.25	2.32	0.43	2.02	0.23	2.45	0.47	2.02	0.23	2.53	0.51
2080	2.02	0.25	2.32	0.43	2.03	0.23	2.45	0.47	2.02	0.23	2.53	0.50
2086	2.02	0.25	2.32	0.43	2.03	0.23	2.45	0.46	2.02	0.23	2.53	0.50
2092	2.03	0.25	2.32	0.43	2.03	0.23	2.45	0.46	2.02	0.23	2.53	0.50
2098	2.03	0.25	2.32	0.42	2.03	0.23	2.45	0.46	2.02	0.23	2.53	0.49

2104	2.03	0.24	2.32	0.42	2.03	0.23	2.45	0.45	2.02	0.22	2.53	0.49
2110	2.03	0.24	2.32	0.42	2.03	0.23	2.45	0.45	2.02	0.22	2.53	0.49
2116	2.03	0.24	2.32	0.42	2.03	0.23	2.45	0.45	2.03	0.22	2.53	0.48
2122	2.03	0.24	2.32	0.41	2.03	0.23	2.45	0.45	2.03	0.22	2.53	0.48
2128	2.03	0.24	2.32	0.41	2.03	0.22	2.45	0.44	2.03	0.22	2.53	0.47
2134	2.04	0.24	2.32	0.41	2.04	0.22	2.45	0.44	2.03	0.22	2.53	0.47
2140	2.04	0.24	2.32	0.41	2.04	0.22	2.45	0.44	2.03	0.22	2.53	0.47
2146	2.04	0.24	2.32	0.40	2.04	0.22	2.45	0.43	2.03	0.22	2.53	0.46
2152	2.04	0.24	2.32	0.40	2.04	0.22	2.45	0.43	2.03	0.22	2.53	0.46
2158	2.04	0.24	2.32	0.40	2.04	0.22	2.45	0.43	2.03	0.22	2.53	0.46
2164	2.04	0.23	2.32	0.40	2.04	0.22	2.44	0.42	2.03	0.21	2.53	0.45
2170	2.04	0.23	2.32	0.39	2.04	0.22	2.44	0.42	2.03	0.21	2.53	0.45
2176	2.04	0.23	2.32	0.39	2.04	0.22	2.44	0.42	2.04	0.21	2.53	0.45
2182	2.04	0.23	2.32	0.39	2.04	0.21	2.44	0.42	2.04	0.21	2.53	0.44
2188	2.05	0.23	2.32	0.39	2.04	0.21	2.44	0.41	2.04	0.21	2.53	0.44
2194	2.05	0.23	2.31	0.39	2.04	0.21	2.44	0.41	2.04	0.21	2.53	0.44
2200	2.05	0.23	2.31	0.38	2.05	0.21	2.44	0.41	2.04	0.21	2.53	0.43

References

1. Chen, X. G., Gu, H. G., Liu, J. M., Chen, C. & Liu, S. Y. Advanced Mueller matrix ellipsometry: Instrumentation and emerging applications. *Science China Technological Sciences 2022 65:9* **65**, 2007–2030 (2022).

2. Fujiwara, Hiroyuki. Spectroscopic ellipsometry : principles and applications. 369 (2007).

3. Knigge, C., Baraffe, I. & Patterson, J. The Lorentz oscillator model. *Essential Classical Mechanics for Device Physics* (2016) doi:10.1088/978-1-6817-4413-1CH5.

4. S., R. Electromagnetic properties of a finely stratified medium. *Soviet Physics JEPT* **2**, 466–475 (1956).

5. Smolyaninov, A., El Amili, A., Vallini, F., Pappert, S. & Fainman, Y. Programmable plasmonic phase modulation of free-space wavefronts at gigahertz rates. *Nature Photonics 2019 13:6* **13**, 431–435 (2019).

6. Kafaie Shirmanesh, G., Sokhoyan, R., Pala, R. A. & Atwater, H. A. Dual-Gated Active Metasurface at 1550 nm with Wide (>300°) Phase Tunability. *Nano Lett* **18**, 2957–2963 (2018).

7. Forouzmand, A. *et al.* Tunable all-dielectric metasurface for phase modulation of the reflected and transmitted light via permittivity tuning of indium tin oxide. *Nanophotonics* **8**, 415–427 (2019).

8. Bennett, B. R. & Soref, R. A. Electro-optic Fabry–Perot pixels for phase-dominant spatial light modulators. *Applied Optics, Vol. 31, Issue 5, pp. 675-680* **31**, 675–680 (1992).

9. Basile, F., Bloisi, F., Vicari, L. & Simoni, F. Optical phase shift of polymer-dispersed liquid crystals. *Phys Rev E* **48**, 432 (1993).

10. Klopfer, E., Dagli, S., Barton, D., Lawrence, M. & Dionne, J. A. High-Quality-Factor Silicon-on-Lithium Niobate Metasurfaces for Electro-optically Reconfigurable Wavefront Shaping. *Nano Lett* **22**, 1703–1709 (2022).

11. Salary, M. M. & Mosallaei, H. Tunable All-Dielectric Metasurfaces for Phase-Only Modulation of Transmitted Light Based on Quasi-bound States in the Continuum. *ACS Photonics* **7**, 1813–1829 (2020).